Incorporation of strontium in earthworm-secreted calcium carbonate granules produced in strontium-amended and strontium-bearing soil

L. Brinza[a,*], P.D. Quinn[a], P.F. Schofield[b], J.F.W. Mosselmans[a], M.E. Hodson[c,1]

[a] Diamond Light Source Ltd., Harwell Science and Innovation Campus, Chilton, Didcot, OX11 0DE, UK

[b] Mineral and Planetary Sciences, Department of Earth Sciences, Natural History Museum, Cromwell Road, London SW7 5BD, UK

[c] Soil Research Centre, Dept. Geography and Environmental Science, School of Human and Environmental Sciences, University of Reading, Whiteknights, Reading, RG6 6DW, UK

* Corresponding author email address: loredana.brinza@diamond.ac.uk (Loredana Brinza)

+44 (0)1235 778517

Running head: Sr in earthworm granules

1. Present Address: Environment Department, University of York, Heslington, York, YO10 5DD, United Kingdom

Abstract

This paper investigates the incorporation of Sr into biomineralized calcium carbonate granules secreted by the earthworm *Lumbricus terrestris.* Experiments were conducted using an agricultural soil amended with $Sr(NO_3)_2$ to give concentrations in the range 50 - 500 mg kg^{-1} Sr and a naturally Sr-rich, Celestine-bearing soil containing up to 11 000 mg kg^{-1} Sr. Granule production rates were in the range 0.26 – 2.3 mg_{CaCO3} $earthworm^{-1}$ day^{-1}; they showed no relationship with soil or soil solution Sr concentration but decreased with decreasing pH. Strong relationships exist ($r^2 \geq 0.8$, $p \leq 0.01$) between the Sr concentrations and Sr / Ca ratios of the granules and those of the soil, soil solution and earthworms. The highest bulk Sr concentration we recorded in the calcium carbonate granules was 5.1 wt% Sr whilst electron microprobe analysis recorded spot concentrations of up to 4.3 wt % Sr. X-ray diffraction and X-ray absorption spectroscopy indicate that the majority of the calcium carbonate is present as Sr-bearing calcite with trace amounts of Sr-bearing vaterite also being present. The granules produced in the Sr-amended soils concentrated Sr relative to Ca from the bulk soil and the earthworms. This suggests that earthworm secreted calcium carbonate may be significant in the cycling of ^{90}Sr released into soils via nuclear accidents or leakage from nuclear waste storage facilities.

1. INTRODUCTION

The incorporation of Sr (and other elements) into calcite and other calcium carbonate phases has been, and continues to be, the subject of much research in the geochemical community (e.g. Bracco et al., 2012; Tertre et al., 2012; DePaolo, 2011; Tang et al., 2008; Lakshtanov and Stipp, 2007; Nehrke et al., 2007; Finch and Allison, 2007; Gabitov and Watson, 2006; Elzinga and Reeder, 2002; Fujita et al., 2004; Parkman et al., 1998; Pingitore et al., 1992; Stipp and Hochella, 1991; Tesoriero and Pankow, 1996). Some of the research is driven by the potential for calcite to immobilise contaminants, particularly ^{90}Sr (e.g. Riley et

al., 1992; Achal et al. 2012; Perdrial et al., 2011; Spycher et al., 2009; Barkouki et al., 2011; Fujita et al., 2010; Tertre et al., 2012). Additionally, the potential use of Sr/Ca ratios in biominerals and speleothems for the reconstruction of past environments is also the subject of numerous studies (e.g. Finch and Allison, 2007; Wassenburg et al., 2012; Sinclair et al., 2012; Bluszcz et al., 2009; Fairchild et al, 2000, Dissard et al., 2010a, 2010b; Stoll et al., 2002). This paper is concerned with Sr partitioning into earthworm-secreted calcite; understanding this system may have important implications for site remediation and environmental reconstruction.

Earthworms are perhaps best known for their role in the breakdown of organic material and the mixing and aeration of soils (Edwards, 2004; Edwards and Bohlen, 1996). However, many species of earthworm also synthesise calcium carbonate (Canti and Piearce, 2003). The calcium carbonate is produced in the calciferous glands as micron-scale spherites which, in many species, go on to coalesce and form millimetre scale granules comprised predominantly of calcite, but also containing aragonite, vaterite and amorphous calcium carbonate (e.g. Canti and Piearce, 2003; Gago-Duport et al., 2008; Lee et al., 2008). The spherites and granules are secreted into the earthworm intestine and, from there, into the soil. Carbon isotope studies of *L. terrestris* granules indicate that the carbon in the granules comes from both carbon dioxide and consumed organic matter (Briones et al., 2008; Canti, 2009). Granule production rates by the earthworm *Lumbricus terrestris* have been linked to soil pH (Lambkin et al., 2011) but the function of the granules is still not clear with suggested functions including Ca, CO_2 and pH regulation in body tissues and fluids (Darwin, 1881, Robertson, 1936; Piearce, 1972).

It is well established that earthworms can accumulate metals when exposed to contaminated or amended soils (e.g. Nahmani et al., 2007). We have shown (Fraser et al., 2011) that, at least for Pb, metals can also accumulate in the calcium carbonate granules secreted by earthworms in those soils; Pb was both structurally incorporated within the calcite in the granules and also present as the Pb-carbonate cerrusite. The Pb-enriched granules contained an unexpectedly large amount of aragonite, consistent with studies

which highlight the influence of various trace elements on calcium carbonate polymorph transformations and stability (e.g., Sr, Mg, Zn, SO_4^{-2}) (Bots et al., 2011; Finch and Allison, 2007; Morse et al, 1997; Reis et al., 2008; Rodriguez-Blanco et al., 2011a; Wang et al., 2012). Morgan et al. (2001, 2002) demonstrated that despite the chemical similarities between Sr and Ca and the accumulation of Sr by earthworms exposed to Sr-rich soils, earthworms are able to metabolically differentiate between Sr and Ca. Studies have shown that the distribution coefficients for Sr incorporation in biosynthesised calcite are up to an order of magnitude higher than values reported in natural and synthetic calcite (e.g. Fujita et al., 2004; Morgan et al., 2001). Strontium 90 is produced by nuclear fission and is a significant component of nuclear waste. It has been accidentally released into numerous environments due to leaks from storage facilities (e.g. Hanford, USA, Thompson et al., 2010; Oak Ridge, USA, Gu et al., 2005; Mayak, Russia, Standring et al., 2002 and Sellafield, UK, Gray et al., 1995) and nuclear accidents (e.g. Fukushima Daiichi). Evidence suggests that the partitioning of Sr into calcite (and other calcium carbonates) is related to environmental variables such as temperature and CO_2 levels; consequently Sr/Ca ratios can be used as a tool for reconstruction of past environments (Fairchild et al., 2000; Dissard et al., 2010a, b).

The aims of the current study were therefore to determine: 1) the extent to which Sr would accumulate in the calcium carbonate produced by *L. terrestris* exposed to Sr-enriched soils, 2) whether distribution coefficients for this incorporation were consistent with those determined for inorganic systems, and 3) whether Sr incorporation impacted on granule mineralogy. Our results are placed in the context of the potential of earthworm calcium carbonate granules within the fields of contaminant immobilisation and environmental reconstruction.

2. METHODS

2.1. Earthworms and soils

Clitellate *Lumbricus terrestris* were obtained from Recycle Works Ltd. (Ribchester, PR3 3XJ, UK). They were kept for one week in a moist mixture of 1:2 by volume peat soil and Kettering Loam (Boughton Loam and Turf Management, Kettering, Northamptonshire, NN16 8UN, UK) prior to being used in the experiments.

Three arable soils were collected for the study, one, Hamble soil (HS) from near Theale, Berkshire OS 164 (SU-618-702) and two Yate soils (Yate Soil High, YSH, and Yate Soil Low, YSL) from the former celestine ($SrSO_4$) mining area of Yate, Bristol OS 172 (ST-712-847) (Nickless et al., 1976).

2.2. Soil characterization

Prior to characterisation and experiment the soils were oven dried (at 40ºC) and sieved to < 250 µm. Subsamples of the soil were dried at 105 °C to remove moisture completely and all results are expressed on a per mass of 105 °C dried soil basis. Selected soil properties are reported in Table 1. Soil water holding capacity (WHC) was determined gravimetrically following ISO 11465:1993 (ISO, 1993). Soil pH in deionised water was determined following BS ISO 10390:2005 (BSI 2005). Loss on ignition (LOI) was determined following BS EN 15935 (BSI 2009) and used as a proxy for organic matter content

Soil elemental composition was determined by aqua regia digest following BS ISO 12914 (BSI, 2010) using an Anton Parr Multiwave 3000 microwave followed by analysis using a Perkin Elmer Optima 7300 DV inductively coupled plasma – optical emission spectrometer ICP-OES). For quality control, an internal reference soil material (SS50) traceable to BCR-143R (Commission of the European Communities, Community Bureau of Reference) and blanks were digested in triplicate. Recoveries were 93% for Ca and 107% for Sr for SS50; repeated analysis of individual samples indicated a precision $\leq$ 0.5 % and detection limits of less than 0.07 mg kg^{-1}.

2.3. Earthworm incubation experiments

Incubation experiments were carried out on the Hamble and Yate soils in a temperature and ventilation controlled Memmert ICP 600 incubator set at 16 °C with minimal ventilation. For the Hamble soil, incubations were carried out on unamended soil (HS) and also Hamble soil to which solutions of anhydrous $Sr(NO_3)_2$ (Sigma-Aldrich, CAS 10042-76-9) were added to give initial target Sr concentrations in soil of 50, 100, 150 and 500 mg Sr kg^{-1} (denoted HS50, HS100, HS150 and HS500, respectively). Higher Sr concentrations (1000 and 4000 mg kg^{-1}) were also used but proved terminal to the earthworms and are not reported here. Amended soils were digested in aqua regia and analysed by ICP-OES to check concentrations. Incubation experiments were carried out in plastic containers enclosed in perforated plastic bags. Each container held 300 mg oven dried soil mixed with either deionised water or $Sr(NO_3)_2$ solution to give a water content of c. 60% of the WHC. An individual *L. terrestris* was weighed and added into each soil sample. Five replicates were run for each concentration.

After 28 days earthworms were removed from the soil, depurated for 48 hours (Arnold and Hodson, 2007), digested by aqua regia and analysed for Sr and Ca by ICP-OES. Detection limits and precision were as reported for the soil digestions. Soil pore water was extracted overnight with 100 mm epoxy bodied MOM Rhizon samplers. pH was measured with a Jenway 3510 pH meter; precision was 0.36 %. Solutions were then acidified with 5% concentrated (≥69%) Sigma-Aldrich nitric acid ACS reagent grade, ISO≥69% (CAS 7697-37-2) prior to analysis by ICP-OES for Ca and Sr. An in house 500 µg kg^{-1} standard gave recoveries of 90 – 110 %. Detection limits were $\leq$ 0.017 mg kg^{-1} and precision was < 2.2%. Soil sub-samples were taken from each incubation for pH measurement (BSI, 2005). The remaining soil was sieved to 500 µm to recover the granules. Granules from each replicate treatment were dried and pooled for weighing to determine production rate expressed as mg $CaCO_3$/g worm/day prior to further characterization.

Two additional incubation experiments were carried out. In one, Hamble soil amended to 500 mg Sr kg^{-1} was incubated but without any earthworm additions. No granules were recovered from this incubation supporting the earthworm-derived origin of the granules.

In the second, granules recovered from our unamended Hamble soil experiment were added to Hamble soil amended to 500 mg Sr kg^{-1} using $Sr(NO_3)_2$. After 28 days the granules were characterised for chemical composition as described in Section 2.4.

2.4. Granule characterization

The majority of granules were dissolved in 5% nitric acid and analysed by ICP-OES. The certified reference material dolomite BCS No386 was also digested following this method and gave a recovery of 117% for Ca. Detection limits were $\leq$ 0.028 mg kg^{-1} with precision of $\leq$ 1.3 %. Remaining granules were used in mineralogical and spatially resolved chemical investigations.

Thin sections of the granules were produced by embedding the granules in EpoFIX (Struers) resin and grinding to a thickness of 50-70 μm, that is, 25-35 μm either side of the granule centre. The granule slices were then mounted on Chance Glass Ltd. glass slides and mechanically polished using a 1 μm particle size corundum slurry.

Bulk granule mineralogy was assessed by combining information gleaned from X-ray powder diffraction (XRD-NHM) on powdered granules and in-house, non-destructive X-ray microdiffraction (μXRD-NHM) on the polished granule sections that were then used for electron probe analysis and X-ray absorption spectroscopy. XRD-NHM data were collected in reflection geometry using a Nonius PDS 120 powder diffraction system consisting of an Inel curved, position sensitive detector (PSD) within a static beam-sample-detector geometry. This system allows the simultaneous measurement of the diffracted X-ray intensities at all angles of 2θ across 120º (Schofield et al., 2002). Cobalt $K\alpha_1$ radiation was selected from the primary beam by a germanium 111 crystal monochromator with the X-ray tube operating at 35 kV and 30 mA. Horizontal and vertical slits restricted the beam to a height of 0.24 mm and width of 4.0 mm. Individual granules were powdered in an agate pestle and mortar, mixed with acetone and thinly deposited on a circular sapphire substrate. NIST silicon powder SRM640 and silver behenate were used as external standards;

194 calibration and data collection were performed using in house software Diffgrab™. Data
195 were collected for a minimum of 2000 s with samples spinning continuously in the plane of
196 the sample surface and with the sample surface at an angle of 4.0º to the incident beam.
197 μXRD-NHM data were collected using a Nonius PDS 120 powder diffraction system as
198 described above. In this case a 100 μm diameter beam was selected by a pinhole from a
199 300 μm diameter primary beam of Cu Kα radiation generated by a GeniX system with a
200 Xenocs FOX2D CU 10_30P mirror operating at 50 kV and 1 mA (Lambiv Dzemua et al.,
201 2012). Measurements were made in reflection geometry. The surface of the granule polished
202 section was brought into the focal point of the beam using a Zeiss Axio Cam MRc5 CCD
203 optical system. The footprint of the beam on the sample was 750-500 × 100 μm. During data
204 collection, the polished sections were spun continuously in the plane of the sample surface.
205 NIST silicon powder SRM640 and silver behenate were used as external standards;
206 calibration and data collection were performed using Diffgrab™ with data collection times of
207 at least 3000 s.

208 Elemental distribution within the granules was mapped using both electron probe
209 microanalysis (EPMA) and synchrotron based X-ray fluorescence (sXRF). EPMA element
210 maps were generated using a Cameca SX100 electron microprobe operating at 15 kV and
211 100 nA with the beam set to a spot size of 1 μm. Wavelength dispersive spectrometers
212 (WDS) were used to detect elements Ca, Sr, Mn, Mg and Fe while the elements Na, Al, Si,
213 P, S, Cl, K and Ti were detected using an energy dispersive spectrometer (EDS). Maps were
214 512 × 512 pixels with step sizes of 4-5 μm and dwell times of 180 – 200 ms.

215 Quantitative electron microprobe chemical analyses of the granules were performed
216 using a WDS Cameca SX100 microprobe operating with 10 kV accelerating voltage, 100 nA
217 beam current, and a spot size of ~20 μm. All elements were analysed using WDS and the
218 probe standards used were: calcite for Ca, celestine for Sr and S, $MnTiO_3$ for Mn, forsterite
219 for Mg, fayalite for Fe, jadeite for Na, corundum for Al, KBr for K, and wollastonite for Si,
220 $ScPO_4$ for P. The X-ray intensities were corrected using a standard PAP correction

procedure. Between 20 and 40 points were analysed on each granule along rim-core-rim line profiles. The atomistic detection limits for Ca, Mg, Sr and Mn were 0.05, 0.02, 0.03 and 0.04 wt %, respectively, and the wt % oxide standard deviations for CaO, MgO, SrO and MnO were 0.5, 0.02, 0.03 and 0.03, respectively.

The sXRF was performed on the microfocus beamline I18 at the Diamond Light Source (Mosselmans et al., 2009) where sXRF maps were collected using a 9-element Ge detector with the Si(111) cryogenically-cooled monochromator set to provide an incident X-ray energy of 16500 eV. The beam-on-sample size was 5 × 5 μm. and maps were collected with 30 μm steps. XRF data were processed in PyMCA 4.4.1 (Solé et al., 2007). sXRF maps were used principally to determine suitable points for microfocus X-ray absorption spectroscopy.

2.4.1. Micro X-ray Absorption Spectroscopy (μXAS)

μXAS was carried out on the thin sections of the granules using the microfocus beamline I18 at the Diamond Light Source. μXAS was carried out on one granule each extracted from HS150, HS500, YSL and YSH and two granules extracted from HS100. For most of the granules two Ca K-edge XANES and Sr K-edge EXAFS spectra were collected from the same point of interest at several different points. Recurrent spectra were compared to check for any sign of beam damage. For all the spectra obtained no changes were seen in these recurrent spectra. XAS data were processed in Athena (Ravel and Newville, 2005) and Pyspline (Tenderholt and Quinn, 2009) and fitted using DL_Excurv (Tomic et al., 2004).

Sr K-edge spectra of relevant standards were recorded as follows: celestine (collected from the Yate soil), $SrCO_3$ (Fisher Scientific), and $Sr(NO_3)_2$ (Fisher Scientific) spectra were obtained in transmission mode using samples ground together with boron nitride and pressed into pellets. Fluorescence data were collected from Sr-containing aragonite (this sample is speleothem aragonite from Makapansgat Valley, South Africa and was provided by Dr. A. Finch, University of St Andrews), calcite with Sr adsorbed onto it,

earthworm-produced calcium carbonate granules with Sr adsorbed onto them and vaterite co-precipitated with Sr.

Calcite for the Sr adsorbed standard was synthesized following the method of Rodriguez-Blanco et al. (2011b). The powder produced had a BET surface area of 0.99 m^2 g^{-1} whilst the granules had a BET surface area of 0.83 m^2 g^{-1}. One gram of either the synthesised calcite or calcium carbonate granules recovered from our unamended Hamble soil experiment was equilibrated in 50 mL of a pH 7.5 solution of $NaHCO_3$ and HCl at 20 °C for 24 hours, the pH adjusted back to 7.5 and then Sr added as $Sr(NO_3)_2$ (Sigma-Aldrich, CAS 10042-76-9) to give a solution concentration of 100 nM Sr per g calcite. After 24 hours the adsorbent was collected via centrifugation.

Vaterite co-precipitated with Sr was made following the method of Bots (2012). A solution of 100 mM $CaCl_2$ was rigorously mixed with a solution of 50 mM Na_2CO_3 and 1.25 M Na_2SO_4 on a magnetic stirring plate. Sr was added to the $CaCl_2$ solution as $Sr(NO_3)_2$ to give a concentration of 100 µM Sr. Vaterite precipitated instantly, was washed by filtration with deionised water to remove sulphate and dried in isopropanol. The precipitate was shown to be pure vaterite using XRD.

An attempt was made to synthesize standards of calcite co-precipitated with Sr following the method of Gruzensky (1967). Solutions of $CaCl_2$ with $SrCl_2$ were prepared to give final Sr concentrations in solution of 100 µM, 1 µM and 10 mM Sr. In each case however the resulting precipitate was a mixture. For solutions of 100 µM, and 1 µM Sr the calcite was precipitated with vaterite while the solution of 10 mM Sr produced calcite with Ca-bearing strontianite and aragonite.

Ca K-edge XANES data were collected in fluorescence mode from the speleothem aragonite and also synthetic vaterite stabilized with 4% sulphate (provided by Dr. P. Bots, University of Leeds). As the Ca XANES data were collected in fluorescence mode the spectra are distorted by self-absorption. Corrections can, in principle, be made for self absorption and a basic example of such a correction is shown for Ca K-edge XANES from a calcite single crystal in the Supplementary Information. In order to make an accurate self-

absorption correction, a knowledge of the density of the sample is required. As the granules of this study have a mineralogy that may vary within the volume of sample analysed at each point, this is not a feasible option. Consequently, no corrections have been applied to the Ca K-edge XANES from the granules in this study, however, as all the spectra were recorded in the same way comparisons between the spectra can be made.

2.5. Statistics

Statistical analysis was carried out using Sigma Stat 3.0.1 by SPSS. All data were checked for normality using the Kolmogorov-Smirnov test before analysis and appropriate parametric or non-parametric statistics used. Soil Sr concentrations were compared using Kruskall-Wallis one way analysis of variance on ranks, changes in earthworm weight during the course of the experiment by one way analysis of variance. Pearson and Spearman's rank correlations were determined as appropriate for relationships between soil, soil solution, earthworm and granule chemistry and granule production.

3. RESULTS AND DISCUSSIONS

3.1. Soil solution

Sr concentrations in the amended Hamble soils varied about the target values potentially due to uncertainties in extraction efficiency and analysis. However, importantly for the present study soils with significantly different Sr concentrations were produced (Table 1, $p \leq 0.01$). The low concentrations of Sr in the soil solution in the YSL and YSH soils relative to the Sr amended Hamble soils (Table 1) reflects the sources of Sr in the soils, celestine in the Yate soils (Nickless et al., 1976) and the more soluble $Sr(NO_3)_2$ in the Sr-amended Hamble soil.

3.2. Earthworm survival and chemistry

No earthworms died over the duration of the experiment but they all lost weight. Average weight loss was 6.4 ± 11.8 % of their body weight (n = 6 ± s.d.). There were no significant differences in weight loss between soils or treatments ($p \geq 0.05$). Earthworm chemistry is summarised in Table 2. The range of Sr concentrations is similar to that reported for different species kept in soils collected from the Yate region by Morgan et al. (2001, 2002) but Ca concentrations are up to an order of magnitude higher. This appears to reflect the higher Ca concentrations in our soils compared to those in Morgan's study (1250 – 5540 mg kg^{-1}). Additionally Morgan et al. (2001) studied different species of earthworms, three of which, *Aporrectodea caliginosa, Aporrectodea longa* and *Allolobophora chlorotica,* have less well developed calciferous glands which produce far fewer granules (Canti and Piearce, 2003) which may impact on Ca accumulation. The concentration of Sr accumulated by earthworms, in this study, increased with the concentration of Sr in the soil ($r^2 = 0.92$, $p \leq 0.05$) and the soil solution ($r^2 = 0.88$, $p \leq 0.05$), but no correlation was found for Ca supporting the conclusion of Morgan et al. (2001) that Ca uptake is regulated whilst Sr uptake is not.

Similarly to Morgan et al. (2001) concentration factors calculated for earthworm body loads using the bulk soil concentrations for Sr and Ca were 0.89 $\pm$ 0.42 and 1.14 $\pm$ 0.45 (mean $\pm$ s.d., n = 32), respectively. Distribution coefficients (D) for Sr and Ca were calculated as the ratio of the Sr/Ca in the earthworm and Sr/Ca in the soil or soil solution and are given in Table 3. On average values for earthworm distribution coefficients are 0.81 $\pm$ 0.31 and 0.51 $\pm$ 0.26 (mean $\pm$ s.d., n = 32) for partitioning between the earthworm and soil and the earthworm and soil solution, respectively, indicating that if uptake and accumulation is from the bulk soil there is no discrimination between Sr and Ca ($D \cong 1$) whereas if uptake is from the metal in solution Ca is preferentially taken up ($D < 1$). For the earthworm – soil distribution coefficients the unamended Hamble soil and the YSL soil have relatively low values presumably reflecting the low Sr content of the unamended Hamble soil and the non-bioavailable nature of the Sr in the YSL soil, respectively.

328 The earthworm – soil solution partition coefficient for YSH is higher than the other
329 values, possibly reflecting the relatively high Sr / Ca ratio of the YSH soil solution. Unlike the
330 findings of Morgan et al. (2001) there is no indication that Sr bioaccumulation decreases
331 relative to Ca at higher soil Ca concentrations. This may reflect the narrower range of Sr and
332 Ca concentrations in our study and the fact that the low Sr concentration soils were
333 amended with highly soluble (and therefore more bioavailable) $Sr(NO_3)_2$ whilst the high Sr
334 concentration soils contained the less soluble (and therefore less bioavailable) celestine.

335

336 **3.3. Granule production, bulk mineralogy and bulk chemistry**

337 Granule production rates (Table 2) were similar to those reported by Fraser et al.
338 (2011) in Pb amended artificial soils and by Lambkin et al. (2011) in agricultural soils . There
339 were no significant correlations between the Sr concentration of the soil or soil solution and
340 granule production rate. The lower production rate recorded for soil YSL is consistent with
341 the reduction in granule production with decreasing pH reported by Lambkin et al. (2011).

342 Analysis of bulk and micro XRD data shows that calcite is the main component of the
343 granules with vaterite often present as well (Table 4). Trace amounts of quartz were
344 identified in all the granules but no Sr-carbonate or Sr-sulphate phases such as strontianite,
345 carbocernaite or celestine were identified. The quartz is potentially incorporated within
346 granules during their transportation from the calciferous glands into oesophageal pouches
347 where the granules are stored before being excreted and where granules growth may still
348 occur (Lee et al., 2008).

349 The bulk concentrations of Sr and Ca in the granules as measured by ICP-OES are
350 reported in Table 2, where it can be seen that substantial levels of Sr are incorporated into
351 the calcium carbonate granules. The concentrations of Sr reported in the granules are high
352 but similar values have been reported in the literature. Concentrations of Sr in inorganically

produced calcite reported in the literature include 8505 mg kg^{-1} (Pingitore et al., 1992), 1477 mg kg^{-1} (Tang et al., 2008) and 1300 – 3500 mg kg^{-1} (Gabitov and Watson, 2006). Concentrations of Sr in biogenic calcite are often higher, with reported concentrations including 27 000 mg kg^{-1} in the common groundwater, gram-positive bacteria, *Bacillus pasteurei*, (Warren et al., 2001, with vaterite also present) and up to 5000 mg kg^{-1} in decapods (Veizer, 1983). EPMA of the granules confirmed the high Sr concentrations within the granules (Table 4). For granules produced in the Hamble soils the granules with the highest SrO levels (up to 5 wt% SrO or 4.3 wt % Sr) are those produced in the soils amended to the highest concentration of Sr. The high concentrations of Sr may in part reflect the crystallisation history of the predominantly calcite granules given that initially the calcium carbonate is amorphous (e.g. Gago-Duport et al. 2008) and that amorphous calcium carbonate can be preserved in the granules (e.g. Lee et al. 2008). Calcite that forms via amorphous calcium carbonate can have elevated Mg concentrations (e.g. Radha et al., 2012; Raz et al, 2000; Wang et al. 2012) and it is possible that similar effects occur for Sr though we are not aware of any published studies on this subject. It should also be noted that the bulk Mg concentrations in the granules are low ($\leq$ 31 mg kg^{-1}) and even narrow bands of high Mg concentration (Table 4) are below the levels found in many biogenic calcites or thought to represent maxima for calcite formed directly from solution rather than from an amorphous precursor (e.g. Berner, 1975, Fernández-Díaz et al., 1996; Loste et al., 2003)

In order to assess the potential for Sr adsorbing to granule surfaces post secretion/excretion granules produced in unamended, Sr-free Hamble soil were placed in Hamble soil amended to 500 mg Sr kg^{-1} for 28 days. Subsequent ICP-OES analyses revealed that Sr levels associated with the granules increased from 345 mg kg^{-1} in the control granules (Table 2) to 1370 mg kg^{-1}. In contrast Sr levels in granules produced by earthworms in Hamble soil amended to 500 mg Sr kg^{-1} were 34200 mg kg^{-1} (Table 2). This

suggests that if Sr adsorption from the soil solution to the granule surface occurs then it only accounts for a small fraction of the total Sr associated with the granules.

As described in detail by Fraser et al. (2011), in X-ray diffraction the calcite 104 peak position is a good indicator of relative changes in the size of the calcite unit cell. Calcite 104 peak positions taken from bulk XRD data are reported in Table 4. In order to ensure that these XRD measurements are compared with appropriate Sr levels in granule calcite, the wt% SrO of each granule was estimated from the average wt% SrO value from EPMA point analyses within a rim-core line profile of large calcite crystals making up the granules (Table 4) rather than using the Sr concentrations measured by ICP-OES (Table 2) which are average values for a range of granules and which will therefore include Sr present in vaterite; however the trends observed are the same regardless of which Sr data are used. Figure 1 shows the calcite 104 peak position as a function of the estimated average wt% SrO from EPMA analyses for the granules produced by earthworms in Hamble soils (and not those produced in Yate soils for which there is no “control” specimen, i.e. granules produced in an equivalent soil but with the absence of Sr). It can been seen that the calcite 104 peak shifts to lower 2θ values as the Sr concentration in the granule calcite increases. A shift of the calcite 104 peak to lower 2θ values is indicative of an increasing unit cell size suggesting that Sr, which is larger than Ca, is structurally incorporated by the calcite.

No aragonite was identified within any of the granules of this study, although the study of Fraser et al. (2011) found granules comprising calcite and aragonite with no vaterite being present. The current study used a natural soil amended with Sr and a natural Sr-rich soil, whereas in the study of Fraser et al. (2011) the biogenic calcium carbonate granules were produced by *L. terrestris* in artificial soil amended with Pb. This suggests that the mineralogy of the calcium carbonate granules may be influenced by soil, consistent with experiments on the inorganic calcium carbonate system (e.g. Bots et al., 2011; Finch and Allison, 2007; Rodriguez-Blanco et al., 2011a). The production of mixtures of different

405 phases when we attempted to co-precipitate calcite with Sr using different concentrations of
406 Sr in solution to produce standards also supports this suggestion.

407 The Sr concentrations and the Sr/Ca ratio of the granules are strongly related ($r^2 \geq$
408 0.8, $p \leq 0.01$) to those of the soil, the soil solution and the earthworms. Distribution
409 coefficients (Table 3) suggest differences in the partitioning of Sr and Ca in the granules
410 between the Sr amended and naturally Sr-rich soils. The partitioning of Sr and Ca from the
411 soil and soil solution is mediated by the earthworm metabolic processes. As such the
412 distribution coefficients reported here cannot be fairly compared with distribution coefficients
413 for Sr and Ca partitioning in inorganic calcite precipitated from solution. However, the values
414 obtained are similar to that of 0.49 obtained for biogenic calcite produced by the bacterium
415 *Bacillus pasteurii,* (Fujita et al., 2004) and greater than many obtained for inorganic calcite
416 (e.g. 0.021 ± 0.003 by Tang et al., (2008) and up to 0.140 by Tesoriero and Pankow, (1996))
417 suggesting that earthworms, like bacteria (Warren et al., 2001), can more efficiently partition
418 Sr into calcite than inorganic processes. Indeed the distribution coefficients for partitioning
419 between the granules and bulk soils suggest that, for the Sr-amended soils, the granules
420 may preferentially concentrate Sr with the granule – earthworm partition coefficients for
421 these soils also suggesting the granules concentrate Sr relative to Ca compared to the
422 earthworm tissues. This finding is consistent with that of Morgan (1981) who found that Sr
423 injected directly into the coelomic cavity of *L. terrestris* in the form of $SrCl_2$ solution was
424 detected in the calciferous glands and spherites within the glands but not in the
425 chloragogenous tissue, an organ associated with the accumulation and metabolism of Ca.

426 The granule-soil and granule-soil solution partition coefficients are similar to those for
427 the earthworm-soil and earthworm–soil solution partition coefficients for the amended soils
428 but are substantially lower for the YSL and YSH soils. The granules have a relatively lower
429 Sr/Ca ratio than the earthworms in the YSL and YSH soils compared to the Sr amended
430 soils. This suggests that the accumulated Sr from the YSL and YSH soils is somehow
431 transported or metabolised differently to that accumulated from the amended soils or has a

different availability due to the soil chemistry. This would be expected given the different forms of Sr present in the soils and is supported by the granule–earthworm partition coefficients which show more partitioning of Sr relative to Ca in the granules compared to the earthworms for the Sr amended soils. Despite the strong correlation between granule and earthworm Sr, the granule-earthworm partition coefficients suggest that after Sr is accumulated in the earthworm the partitioning of Sr into granules via the calciferous gland is not a straight forward process dependent solely on Sr concentrations. For example the distribution coefficient decreases with increasing earthworm Sr/Ca ($r^2 = 0.69$, $p \leq 0.05$) perhaps suggesting that at higher Sr/Ca ratios there is preferential excretion of Sr preventing its partitioning into the granules or that the transport path of Sr to the granules is saturated (Chwodhury et al., 2000; Dodd, 1967). Alternatively this may reflect a precipitation rate effect. In inorganic systems higher rates of calcite precipitation result in greater partitioning of Sr into calcite (e.g. Nehrke et al., 2007; Tang et al., 2008; Tesoriero and Pankow, 1996; Gabitov and Watson, 2006). Granule production rates are lower in the YSL and YSH soils than in the HS soils perhaps suggesting a lower precipitation rate of calcite in the earthworm calciferous glands and a consequent reduction in the partitioning of Sr into the calcite. This also raises the possibility that the apparent preferential partitioning of Sr into biogenic calcite compared to inorganic calcite discussed above may be due to precipitation kinetics.

The potential difference in partitioning of Sr to the granules between the amended and non-amended soils suggests that further investigation is warranted. As such we carried out spatially resolved studies to determine the compositional and crystallographic distribution of Sr in the granules.

3.4. Sr distribution within granules

456 The internal structure of granules has been well described by Lee et al. (2008), and
457 in this study comprises two distinct types, with each type being found in granules extracted
458 from all the different treatments used in this study. The first type comprise a densely
459 compact aggregate of >30 μm carbonate crystals whose orientations appear to be consistent
460 (often radial) within individual layers (e.g. Fig. 2a). These granules are made up of only a few
461 distinct layers. The second type are silicate-inclusion rich and comprise several concentric
462 rings that are poorly linked together and are interspersed with large void spaces. The
463 carbonate crystals within these types of granules are generally smaller than those of the
464 more dense granules (e.g. Fig. 2b).

465 EPMA element maps of the granules from Hamble soils all show concentric
466 zoning of Sr, Mg and Mn. Similar zoning has been observed previously in granules produced
467 by *L. terrestris* in Hamble soil using cathodoluminescence and SEM imaging (Lee et. al.,
468 2008). There is no relationship between type of zoning and the different granule
469 morphologies described above. In general the concentric rings for the Sr were broad in
470 nature. However, there appears to be no consistency to the zoning within the granules either
471 across the study or within individual experiments / Sr amendments (Fig. 3). Some granules
472 from the Hamble soils showed Sr-rich cores and rims, some granules showed Sr-rich cores
473 and Sr-poor rims, and some granules showed Sr-poor cores with Sr-rich rims.

474 In contrast to the Sr, the concentric rings for Mg were generally very narrow and
475 distinct (Fig. 4) reflecting relatively large changes in Mg concentration (Table 4). This wide
476 range in Mg concentrations suggests that, unlike various other organisms (e.g. Bentov and
477 Erez, 2006; Lorens and Bender, 1977; Wang et al., 2012) there is no biotic control on the Mg
478 content of the earthworm-produced calcite. There appears to be no consistency between the
479 granules regarding the number, frequency or radial position of the Mg rich rings. The zoning
480 of the Mn within the granules was generally more diffuse than that for Sr and Mg, and the
481 concentric nature of the zoning showed broad bands rather than the ring structure displayed

by Mg. The Mn zoning patterns within the granules had far more consistency than for Sr and Mg with granules from the same experiment displaying the same basic distribution of Mn-rich and Mn-poor bands.

Statistical correlations between Ca, Sr, Mg and Mn were determined for both the EPMA element maps and the quantitative point analyses across the rim-core-rim line profiles. No significant correlations exist between any pair of elements.

Barker and Cox (2011) showed that laboratory synthesized inorganic calcite co-precipitated with rare earth elements shows the same style of zoning as that observed in the granules strongly suggesting that inorganic processes are responsible for the granule zoning. The zoning is likely due to episodic elemental enrichment of the fluid surrounding the granules and the subsequent incorporation of the enriched elements in the growing granules. These fluctuations in concentration may be due to the composition of soil and soil solution that the earthworm encounters at any given moment in time. Alternatively, or additionally, they may be due to the incorporation of the trace elements into the granules being more rapid than their replenishment at the granule growth front by diffusion through the fluid in the calciferous gland; over time the concentration of the granule-incorporated element would again increase in the fluid leading to its renewed incorporation into the granule (Shore and Fowler, 1996). The apparent inconsistency in the zonation pattern for granules within the same experiment may be due to changes over time in the chemistry of the fluid from which the granules precipitate. In addition the elemental zoning may relate to changes in the mechanism or pathway of the calcium carbonate formation reaction with elemental enrichment being associated with the behaviour of potential precursor phases such as amorphous calcium carbonate and/or vaterite.

The granules produced by *L. terrestris* in the Yate soil showed a different pattern of elemental zoning. Sr was only present in a 5 – 60 μm wide zone around the rim of the YSL granules and only present in ~200 μm diameter patches of microcrystalline calcium

carbonate in YSH granules. The zonation pattern for Mg within the YSL and YSH granules was the same as that for the granules from Sr amended Hamble soil, while Mn showed no zoning pattern in YSH and a small enriched rim in the YSL granules that correlated with the zoning shown by Sr. These differences may reflect differences in the speciation of these elements, and hence their availability for uptake, between the amended and naturally Sr-rich soils. However, none-with-standing the large range of Mg values shown in the zoning mitigating against a biological control over the Mg content of the calcite, the similarity in the Mg zoning between the HS and YSL and YSH granules may somehow reflect the biological origins of the granules.

3.5. Sr and Ca μXAS of the granules

3.5.1. Ca K-edge XANES

The Ca XANES spectra of the calcium carbonate standards and representative spectra obtained from granules recovered from the experiments are shown in Figure 5. For the HS granules we only present spectra obtained from a granule extracted from HS100 as these are typical of the spectra obtained from the granules extracted from the other HS soils, which themselves are presented in the Supplementary Information. Also given in the Supplementary Information are spectra from other points analysed on granules extracted from YSL and YSH.

The Ca XANES spectrum of the calcite standard has a pre-edge feature with two peaks at 4.039 and 4.042 keV (marked “1” and “2” in Fig. 5) compared to the other standards which show only one peak in the pre-edge. This pre-edge feature has previously been highlighted by Lam et al. (2007) and Gebauer et al. (2010) and can be used to differentiate calcite from vaterite or aragonite. The vaterite Ca-XANES spectrum in Fig. 5 is

533 similar to vaterite spectra previously reported in the literature (Bots, 2012; Gebauer et al.,
534 2010; Hayakawa et al., 2008; Lam et al., 2007). This spectrum has a single broad peak as a
535 pre-edge feature at 4.040 keV and two broad post edge peaks at 4.048 keV (marked "3" in
536 Fig. 5) and 4.056 keV (marked "4" in Fig. 5) and these two features can be used to
537 differentiate between vaterite and aragonite.

538 Typical Ca XANES spectra obtained from the granules are shown in Fig. 5. The majority of
539 the spectra (43 out of 45) obtained from granules recovered from the amended Hamble soils
540 from which granules were analysed (e.g. HS100 point A and B), all 6 spectra obtained from
541 granules recovered from YSL (e.g. YSL Point A) and 6 of the 10 spectra obtained from
542 granules recovered from YSH (e.g. YSH Point A) are similar to the calcite Ca K-edge
543 XANES spectrum (Fig. 5). The structural motif of the diagnostic pre- and post-edge features
544 at c. 4.048 eV and 4.060 eV are the same in all these specta, and thus confirm that these
545 granules are mostly calcitic in nature. Small differences in the post-edge region of these
546 spectra exist, specifically in the shape of the main peak and the broadness of the second
547 oscillation, which are similar to those described in our earlier study of Pb in earthworm
548 granules (Fraser et al., 2011). As described earlier, the granules predominantly comprise
549 large single crystals of calcite with respect to the size of the microbeam and thus each
550 spectrum is likely to be associated with one individual calcite crystal. Consequently, the
551 small differences observed in these spectra are probably due to differences in the orientation
552 of the calcite crystals with respect to the polarised nature of the X-ray beam (see
553 Supplementary Information for more detail). Some of the differences observed between
554 these spectra, however, may be the result of electronic or crystal-structure changes induced
555 by structural incorporation of Sr or Mn into the calcite lattice. The other two Ca XANES
556 spectra from granules recovered from Hamble soil (i.e. 2 of the 45 spectra) are indicative of
557 mainly vaterite and are represented on Fig 5 by the spectrum labelled HS100 Point C. The
558 remaining 4 spectra obtained from granules recovered from YSH (e.g. YSH Point B in Fig. 5)
559 are also indicative of vaterite. The difference in the pre-edge region between the two

560 polymorphs is clearly shown in the difference in the derivative spectra near 4.039 keV shown
561 in the inset of Fig 5.

562 Hence the Ca K-edge XANES analysis only indicates the presence of two calcium
563 carbonate phases. It should be noted that the attenuation length for X-rays just after the Ca
564 K-edge in calcite is around 8 microns, thus each XANES spectrum is from c. 200 μm^3 of the
565 sample. As XAS is an averaging technique, phases that are present at less than about 10
566 volume% will be difficult to identify. We see calcite XANES for nearly all the points sampled
567 in granules obtained from both the Hamble and YSL soils with only an occasional spectrum
568 of vaterite from a Hamble soil granule. Thus, in agreement with the XRD results (Table 4),
569 we conclude calcite is the dominant phase for the HS and YSL granules with vaterite a
570 minority phase in the HS granules. Ca K-edge XANES for granules extracted from YSH
571 indicated the presence of both calcite (YSH Point A, Fig. 5) and vaterite (YSH Point B, Fig.
572 5), with vaterite XANES being recorded more frequently than in the granules from the other
573 soils. Again the Ca K-edge XANES are in broad agreement with the XRD results (Table 4)
574 whereby the mineralogy of the YSH granules is mostly calcite with additional vaterite.

575

576 **3.5.2. Sr K-edge XANES and EXAFS**

577 Sr K-edge XANES spectra recorded from the Sr standards and typical Sr K-edge
578 XANES from the granules are shown in Fig. 6. All the Sr K-edge XANES spectra collected
579 from different granules are presented in the Supplementary Information. The majority of the
580 Sr K-edge XANES spectra resemble the spectra of our standards “Sr adsorbed onto calcite”
581 and “Sr adsorbed onto granule” (Fig. 6), though some small differences are evident in the
582 intensity of the shoulder (or first oscillation) on the high energy side of the white line at c.
583 16.122 keV. As described for such differences observed between the Ca K-edge XANES
584 spectra, these slight variations are probably related to the orientation of the sample with
585 respect to the polarization of the X-ray beam. The Sr K-edge XANES spectra in Fig. 6 for the

586 granules recovered from the soils (except YSH Point B) and the 2 standards for Sr adsorbed
587 onto calcite and granules are very similar to those previously reported in the literature for Sr
588 structurally incorporated into the calcite lattice (Pingatore et al., 1992; Parkman et al., 1998;
589 Fujita et al., 2004; Finch and Allison, 2007). This suggests that during the preparation of our
590 standards “Sr adsorbed onto calcite” and “Sr adsorbed onto granules” Sr has become
591 structurally incorporated into the calcite lattice, either through diffusion or via a dissolution re-
592 precipitation mechanism (Lakshtanov and Stipp, 2007; Stipp and Hochella, 1991; Tang et
593 al., 2008; Tesoriero and Pankow, 1996). Furthermore, it suggests that in the majority of our
594 granules the Sr is structurally bound within the calcite lattice.

595 Some of the Sr K-edge XANES spectra obtained from granules extracted from the
596 YSH soil (i.e. 5 of the 11 spectra) appear to show significant differences to the majority of the
597 Sr K-edge XANES spectra; these spectra are represented in Fig. 6 by spectrum YSH Point
598 B. They are similar both in appearance and also in terms of the energy shift of the white line
599 with respect to the other spectra of Fig. 6 to the Sr K-edge XANES spectrum of the
600 inorganically synthesised Sr co-precipitated vaterite standard. Thus we assign them to Sr
601 structurally incorporated into vaterite, an interpretation supported by the Ca K-edge XANES
602 and XRD results.

603 Of all the Sr K-edge EXAFS spectra from the granules, 34 out of the 35 spectra
604 obtained from 5 different granules produced in the different Sr-amended Hamble soil (e.g.
605 HS100 Points A and B, Fig. 6), all 5 spectra obtained from granules produced in YSL (e.g.
606 YSL Point A, Fig. 6) and 6 of the 11 spectra obtained from granules produced in YSH (e.g.
607 YSH Point A, Fig. 6) look very similar to each other and also to the EXAFS of our standards
608 “Sr adsorbed on calcite” and “Sr adsorbed on granules”. These spectra were collected from
609 the same points for which the Sr K-edge XANES spectra were collected, and which
610 suggested that the Sr was structurally bound within the calcite. Pingatore et al. (1992)
611 suggested a model for Sr within the calcite lattice in which the first 3 shells comprise six O

atoms, six C atoms and six Ca atoms, respectively. This model, which reflects well the crystal structure reported by Effenberger et al. (1981), also represents the best fit to the Sr K-edge EXAFS spectra for these points whereby Sr is surrounded by six O atoms at a distance of 2.52 Å, followed by a six C atoms and six Ca atoms at a distance of c. 3.33 Å and c. 4.09 Å, respectively (see Table 5).This is the model for incorporation into calcite used by Elzinga and Reeder (2002) in their studies of other elements. It differs from the models used by Parkman et al. (1992) and Finch and Allison (2007), in that they use a shell occupancy of 3 for C in the second coordination shell. However the Sr-C and Sr-Ca distances in our model are similar to those reported in both of those studies.

The Sr^{2+} ion is substantially bigger than the Ca^{2+} ion with a six-coordinate ionic radius of 1.21 Å compared with 1.00 Å for Ca (Shannon, 1976) and thus it is expected that the calcite lattice would be locally expanded around a substituting Sr. We find a Sr-O bond distance of c. 2.51 Å compared to 2.36 Å for Ca-O in calcite (Effenberger et al., 1981). The Sr-EXAFS data from granules obtained in HS soils indicates that Sr replaces Ca in the calcite lattice with a local structural distortion of +7.2% for Ca-O bond lengths and +3.4% for Ca-C distances, respectively. For comparison, Finch and Allison (2007), quantified a 6.5% local dilation in the calcite structure as a consequence of the Sr substitution.

The Sr substitution into calcite model fits the Sr data at HS100 Point C (Fig. 7); at the same point the Ca K-edge XANES indicated the presence of vaterite (Fig. 5). This apparent discrepancy is due to differences in the sampling volume for Ca and Sr XAS. The attenuation length of X-rays at the Sr K-edge (16.1 keV) in calcium carbonate is c. 350 µm, while just after the Ca K-edge (4.05 keV) it is only 8 µm. Thus the Sr EXAFS will be from the whole granule slice thickness while the Ca XANES represents only the top 8 µm or so. Consequently, while the Ca K-edge XANES data is from vaterite which dominates the outer 8 µm of the sample, the Sr K-edge XAS data is from both this vaterite and also from underlying calcite. As the calcite is the dominant phase in the sampled volume the Sr K-edge

638 EXAFS data can be well fitted by the Sr in calcite model. Indeed, the spectrum presented in
639 Fig. 7 has some features that appear to be part way between those of Sr in calcite and those
640 of YSH point B (see below).

641 Although the Sr in calcite model fitted well 6 of the 11 spectra collected from granules
642 produced in YSH, the other 5 spectra resemble YSH Point B in Fig. 7 and these spectra are
643 better fit by another model; (Sr with 8.5 O atoms at 2.55 Å, 5.2 C atoms at 2.95 Å and then
644 3.5 Ca atoms at 4.13 Å; Table 5). This model is the same as that for our standard vaterite
645 co-precipitated with Sr (Table 5). The precise nature of the vaterite crystal structure is still
646 under debate (Demichelis et al., 2012; Kamhi, 1963; Meyer, 1969; Meyer, 1960), but
647 nevertheless it appears that the radial distribution of atoms about the Ca in vaterite is more
648 complex than that of calcite. The "standard" crystallographic model for vaterite (e.g. Kamhi,
649 1963) has Ca-O, Ca-C, Ca-C and Ca-Ca interatomic distances of 2.28 Å, 2.96 Å, 3.32 and
650 4.24 Å, respectively. Ca-XAS results of Becker et al. (2003) on biogenic vaterite showed a
651 vaterite model with distances of 2.37 Å for Ca-O, 3.09 Å for Ca-O or Ca-C and 4.24 Å for Ca-
652 Ca. Due to the disordered nature of the vaterite crystal structure with respect to that of
653 calcite (e.g. Demichelis et al. 2012), authors of Ca-EXAFS studies have been cautious
654 interpreting or fitting shells and quantifying coordination numbers between 2.9 Å and 3.8 Å
655 (Becker et al., 2003; Demichelis et al., 2012; Lam et al., 2007), but it is generally agreed that
656 Ca-O and Ca-Ca distances of 2.37 Å and 4.24 Å, respectively are characteristic of vaterite.
657 Taking into account the size difference between Sr and Ca our Sr K-edge EXAFS results on
658 Sr incorporation into vaterite are in broad agreement with the existing Ca-XAS data on
659 biogenic and inorganically synthesised vaterite (Becker et al., 2003; Lam et al., 2007),
660 strongly suggesting that Sr can substitute for Ca in the vaterite structure. Furthermore, this
661 study provides evidence of this occurring in inorganically synthesized vaterite as well as
662 vaterite biogenically produced by the earthworm *Lumbricus terrestris*.

663

4. CONCLUSIONS

Granules of calcium carbonate secreted by the earthworm *Lumbricus terrestris* in Sr-rich soils, both those amended with Sr in the form of $Sr(NO_3)_2$ and those that are naturally Sr-rich due to mineralisation, are predominantly calcite with minor amounts of vaterite. In contrast to our previous experiments in which granules were produced in Pb-rich soils (Fraser et al., 2011) no aragonite was found; nor did we detect vaterite in our Pb-rich granules. These findings suggest that the chemistry of the soil or soil solution that the earthworms are exposed to influences granule mineralogy. However, we detected no systematic differences in granule mineralogy across the soils investigated in this study despite their significantly different Sr contents.

The mode of incorporation of Sr in the granules appears to differ from that of Pb in our previous study. Pb was concentrated around granule edges and was predominantly adsorbed to the granule surface prior to secretion of the granules with smaller amounts present either as Pb in calcite or cerussite. Sr is incorporated throughout the granules giving rise to oscillatory zoning with no Sr-carbonate phase being detected. This reflects the increased incorporation of Sr into the calcite lattice by comparison to that observed for Pb (Fraser et al., 2011).

The Sr content of the granules was at the high end of concentrations in calcite previously reported in the literature; distribution coefficients for the partitioning of the Sr into the granules were relatively high compared to those reported for inorganic systems. This may reflect a kinetic effect such as those reported in inorganic systems (e.g. Nehrke et al., 2007; Tang et al., 2008; Tesoriero and Pankow, 1996; Gabitov and Watson, 2006) with the distribution coefficients being lowest for soils in which granule production was also the lowest. The distribution coefficients indicate that, despite their chemical similarities, earthworms are able to metabolically differentiate between Ca and Sr, both in terms of

689 uptake from the soil and incorporation into the calcium carbonate granules which they
690 produce.

691 Whilst granules are unlikely to concentrate Sr from the soil solution relative to Ca, or
692 concentrate Sr from the bulk soil relative to Ca in naturally Sr-rich soils, our results show that
693 if a soil were to experience a significant increase in its Sr concentration, for example by the
694 accidental release of a ^{90}Sr-rich fluid, calcium carbonate granules could accumulate Sr
695 relative to Ca from both the bulk soil and from earthworms. Thus earthworm secreted
696 calcium carbonate granules may have a role to play in the movement of ^{90}Sr in terrestrial
697 ecosystems.

698 Granules have been shown to survive thousands of years in the soil (e.g. Canti,
699 2007), The use of granules as a record of palaeotemperatures is currently being explored
700 (Versteegh et al., 2012). Our findings, that Sr substitutes into the granules with minimal
701 modification of the calcite structure is encouraging for its use as a palaeoproxy. However the
702 use of soil-based mineral palaeoproxies is fraught with difficulty due to the heterogeneity of
703 soils. Much further work on the impact of soil chemistry and temperature on the partitioning
704 of Sr into earthworm secreted calcium carbonate would be required before the full potential
705 of granule trace element chemistry as a palaeoproxy can be assessed.

706

707 **ACKNOWLEDGEMENTS**

708 We thank the Diamond Light Source for the provision of beamtime under grant
709 NT2000. We are grateful to Dr Adrian Finch (University of St. Andrews) and Dr Pieter Bots
710 (University of Leeds) for sharing their standards with us. We thank Dr Tina Geraki (Diamond
711 Light Source) for help with aspects of the data analysis and Anne Dudley (University of
712 Reading) for assistance with the ICP-OES analysis.

713

714 **REFERENCES**

715 Achal V.Pan X. and Zhang D. (2012) Bioremeidation of strontium (Sr) contaminated aquifer
716 quartz sand based on carbonate precipitation induced by Sr resistant Halomonas sp.
717 *Chemosphere* **89**, 764-768.

718 Arnold, R. E. and Hodson, M**.** E. (2007) Effect of time and mode of depuration on tissue
719 copper concentrations of *Eisenia andrei*, *Lumbricus rubellus* and *Lumbricus*
720 *terrestris*. *Environmental Pollution* **148**, 21–30.

721 Barker S. L. L. and Cox S. F. (2011) Oscillatory zoning and trace element incorporation in
722 hydrothermal minerals: insights from calcite growth experiments. *Geofluids* **11**, 48-
723 56.

724 Barouki T.H., Martinez B.C., Mortensen B.M., Weathers T.S., DeJong J.D. Ginn T.R.,
725 Spycher N.F., Smith R.W. and Fujita Y. (2011) Forward and inverse bio-geochemical
726 modelling of microbially induced calcite precipitation in half-meter column
727 experiments. *Transport in porous media* **90** Special Issue, 23-39

728 Becker A., Bismayer U., Epple M., Fabritius H., Hasse B., Shi J. and Ziegler A. (2003)
729 Structural characterisation of X-ray amorphous calcium carbonate (ACC) in sternal
730 deposits of the crustacea Porcellio scaber. *Dalton Transactions* 551-555.

731 Bentov, S. and Erez, J. (2006) Impact of biomineralization processes on the Mg content of
732 foraminiferal shells: A biological perspective. *Geochemistry, Geophysics,*
733 *Geosystems*, **7**, doi:10.1029/2005GC001015.

734 Berner, R.A. (1975) The role of magnesium in the crystal growth of calcite and aragonite
735 from sea water. *Geochemica et Cosmochimica Acta*, **39**, 489-504.

736 Bluszcz P., Lucke A., Ohlendorf C. and Zolitchka B. (2009) Seasonal dynamics of stable
737 isotopes and element ratios in authigenic calcites during their precipitation and
738 dissolution, Sacrower See (northeastern Germany). *Journal of Limnology* **68** 257-
739 273.

740 Bots P. (2012) Experimental investigations of calcium carbonate mineralogy in past and
741 present oceans. Unpublished PhD Thesis, The University of Leeds.
742 Bots P., Benning L. G., Rickaby R. E. M. and Shaw S. (2011) The role of SO_4 in the switch
743 from calcite to aragonite seas. *Geology* **39**, 331-334.
744 Bracco J.N., Grantham M.C. and Stack A.G. (2012) Calcite growth rates as a function of
745 aqueous calcium-to-carbonate ratio, saturation index, and inhibitor concentration:
746 Insight into the mechanism of reaction and poisoning by strontium. *Crystal Growth*
747 *and Design* **12**, 3540-3548.
748 Briones M. J. I., Ostle N. J. and Piearce T. G. (2008) Stable isotopes reveal that the
749 calciferous gland of earthworms is a CO_2-fixing organ. *Soil Biology and Biochemistry*
750 **40**, 554-557.
751 BSI (2005) ISO 10390:2005 Soil quality. Determination of pH. British Standards Online.
752 BSI (2009) BS EN 15935. Soil, sludge, waste, and treated biowaste. Determination of loss
753 on ignition. British Standards Online.
754 BSI (2010) ISO 12914. Soil quality. Microwave-assisted extraction of the aqua regia soluble
755 fraction for the determination of elements. British Standards Online.
756 Canti M. G. and Piearce T. G. (2003) Morphology and dynamics of calcium carbonate
757 granules produced by different earthworm species: *The 7th international symposium*
758 *on earthworm ecology, Cardiff, Wales, 2002. Pedobiologia* **47**, 511-521.
759 Canti M. G. (2009) Experiments on the origin of ^{13}C in the calcium carbonate granules
760 produced by the earthworm *Lumbricus terrestris*. *Soil Biology and Biochemistry* **41**,
761 2588-2592.
762 Canti M.G. (2007) Deposition and taphonomy of earthworm granules in relation to their
763 interpretative potential in Quaternary stratigraphy. *J. Quatern. Sci.* **22**, 111-118.
764 Chwodhury M. J., van-Ginneken L. and Blust R. (2000) Kinetics of waterborne strontium
765 uptake in the common carp., Cyprinus carpio, at different calcium levels.
766 *Environmental Toxicological and Chemistry* **19**, 622-630.

767 Darwin C. R. 1881. *The formation of vegetable mould, through the action of worms, with*
768 *observations on their habits.* John Murray, London
769 Demichelis R., Raiteri P., Gale J. D. and Dovesi R. (2012) A new structural model for
770 disorder in vaterite from first-principles calculations. *CrystEngComm* **14**, 44-47.
771 DePaolo D.J. (2012) Surface kinetic model for isotopic and trace element fractionationduring
772 precipitation of calcite from aqueous solutions. *Geochimica et Cosmochimica Acta*
773 **75**, 1039-1056.
774 Dissard D., Nehrke G., Reichart G and Bijma J. (2010a) The impact of salinity on the Mg/Ca
775 and Sr/Ca ratio in the benthic foraminifera *Ammonia tepida*: Results from culture
776 experiments. *Geochimica et Cosmochimica Acta* **74** 928-940.
777 Dissard D., Nehrke G., Reichart G and Bijma J. (2010b) Impact of seawater pCO2 on
778 calcification and Mg/Ca and Sr/Ca ratios in benthic foraminifera calcite: results from
779 culturing experiments with *Ammonia tepida*. *Biogeosciences* **7**, 81-93.
780 Dodd J. (1967) Magnesium and strontium in calcareous skeletons: A review. *Journal of*
781 *Palaeontology* **41**, 131-1329.
782 Edwards C. A. (2004) Earthworm Ecology. CRC Press, Boca Raton, Florida.
783 Edwards C. A. and Bohlen P. J. (1996) *Biology and Ecology of Earthworms*. Chapman &
784 Hall, London.
785 Effenberger H., Mereiter K. and Zemann J. (1981) Crystal structure refinements of
786 magnesite, calcite, rhodochrosite, siderite, smithonite, and dolomite, with discussion
787 of some aspects of the stereochemistry of calcite type carbonates. *Zeitschrift fur*
788 *Kristallographie* **156**, 233-243.
789 Elzinga E. J. and Reeder R. J. (2002) X-ray absorption spectroscopy study of Cu^{2+} and Zn^{2+}
790 adsorption complexes at the calcite surface: Implications for site-specific metal
791 incorporation preferences during calcite crystal growth. *Geochimica et Cosmochimica*
792 *Acta* **66**, 3943-3954.
793 Fairchild I.J., Borsato A., Tooth A.F., Frisia S., Hawkesworth C.J., Huang Y., McDermott F.
794 and Spiro B. (2000). Controls on trace element (Sr–Mg) compositions of carbonate

795 cave waters: implications for speleothem climatic records. *Chemical Geology* **166**,
796 255–269.
797 Fernández-Díaz, L., Putnis, A., Prieto, M. and Putnis, C. (1996) The role of magnesium in
798 the crystallization of calcite abd aragonite in a porous medium. *Journal of*
799 *Sedimentary Research*, **66**, 482-491.
800 Finch A. A. and Allison N. (2007) Coordination of Sr and Mg in calcite and aragonite.
801 *Mineralogical Magazine* **71**, 539-552.
802 Fraser A., Lambkin D. C., Lee M. R., Schofield P. F., Mosselmans J. F. W. and Hodson M.
803 E. (2011) Incorporation of lead into calcium carbonate granules secreted by
804 earthworms living in lead contaminated soils. *Geochimica et Cosmochimica Acta* **75**,
805 2544-2556.
806 Fujita Y., Taylor J.L., Wendt L.M., Reed D.W. and Smith R.W. (2010) Evaluating the
807 potential of native ureolytic microbes to remediate a Sr-90 contaminated
808 environment. *Environmental Science and Technology* **44** 7652-7658.
809 Fujita Y., Redden G. D., Ingram J. C., Cortez M. M., Ferris F. G. and Smith R. W. (2004)
810 Strontium incorporation into calcite generated by bacterial ureolysis. *Geochimica et*
811 *Cosmochimica Acta* **68**, 3261-3270.
812 Gabitov R. I. and Watson E. B. (2006) Partitioning of strontium between calcite and fluid.
813 *Geochemistry, Geophysics, Geosystems* **7**,12.
814 Gago-Duport L., Briones M., Rodríguez J. and Covelo B. (2008) Amorphous calcium
815 carbonate biomineralization in the earthworm's calciferous gland: pathways to the
816 formation of crystalline phases. *Journal of Structural Biology* **162**, 422-35.
817 Gebauer D., Gunawidjaja P. N., Ko J. Y. P., Bacsik Z., Aziz B., Liu L., Hu Y., Bergström P.
818 L., Tai C.-W., Sham T.-K., Edén D. M. and Hedin N. (2010) Proto-Calcite and Proto-
819 Vaterite in Amorphous Calcium Carbonates. *Angewandte Chemie International*
820 *Edition* **49**, 8889-8891.
821 Gray J., Jones S. R. and Smith A. D. (1995) Discharges to the environment from the
822 Sellafield site, 1951-1992. *Journal of Radiological Protection* **15**, 99-131.

823 Gruzensky P. M. (1967) Growth of calcite crystals. In: Peiser, H. S. (Ed.),*Crystal Growth*.
824 Pergamon, Oxford.
825 Gu B. H., Wu W. M., Ginder-Vogel M. A., Yan, H., Fields M. W., Zhou J., Fendorf S., Criddle,
826 C.S. and Jardine P.M. (2005). Bioreduction of uranium in a contaminated soil
827 column. *Environmental Science and Technology* **39**, 4841-4847.
828 Hayakawa S., Hajima Y., Qiao S., Namatame H. and Hirokawa T. (2008) Characterization of
829 Calcium Carbonate Polymorphs with Ca K Edge X-ray Absorption Fine Structure
830 Spectroscopy. *Analytical Sciences* **24**, 835-837.
831 ISO (1993) ISO 11465:1993, Soil quality *Determination of dry matter and water content on a*
832 *mass base - Gravimetric method*, ISO.
833 Kamhi S. (1963) On the structure of vaterite $CaCO_3$. *Acta Crystallographica* **16**, 770-772.
834 Lakshtanov L. Z. and Stipp S. L. S. (2007) Experimental study of nickel(II) interaction with
835 calcite: Adsorption and coprecipitation. *Geochimica et Cosmochimica Acta* **71**, 3686-
836 3697.
837 Lam R. S. K., Charnock J. M., Lennie A. and Meldrum F. C. (2007) Synthesis-dependant
838 structural variations in amorphous calcium carbonate. *CrystEngComm* **9**, 1226-1236.
839 Lambiv-Dzemua G., Gleeson S. A. and Schofield P. F. (2012) The importance of lithiophorite
840 over asbolane in the ore zone mineralogy of the Nkamouna Co-Mn laterite deposit,
841 southeast Cameroon. *Mineralium Deposita* submitted.
842 Lambkin D. C., Gwilliam K. H., Layton C., Canti M. G., Piearce T. G. and Hodson M. E.
843 (2011) Production and dissolution rates of earthworm-secreted calcium carbonate.
844 *Pedobiologia,* **54**, S119-S129.
845 Lee M. R., Hodson M. E. and Langworthy G. (2008) Earthworms produce granules of
846 intricately zoned calcite. *Geology* **36**, 943-946.
847 Lorens, R.B. and Bender, M.L (1977) Physiological exclusion of magnesium from *Mytilus*
848 *edulis* calcite. *Nature*, **269**, 793-794.

849 Loste, E., Wilson, R.M., Seshadri, R. and Meldrum, F.C. (2003) the role of magnesium in
850 stabilising amorphous calcium carbonate and controlling calcite morphologies.
851 *Journal of Crystal Growth*, **254**, 206-218.
852 Meyer H. (1960) Ueber Vaterit und seine Struktur. *Fortschritte der Mineralogie* **38**, 186-187.
853 Meyer H. (1969) Struktur und fehlordnung des vaterits. *Zeitschrift fuer Kristallographie,*
854 *Kristallgeometrie, Kristallphysik, Kristallchemie (-144,1977)* **128**, 183-212.
855 Morgan A.J. (1981) A morphological and electron-microprobe study of the inorganic
856 composition of the mineralized secretory products of the calciferous gland and
857 chloragogenous tissue of the earthworm, *Lumbricus terrestris* L. The distribution of
858 injected strontium. *Cell and Tissue Research* **220**, 829-844.
859 Morgan J. E., Richards S. P. G. and Morgan A. J. (2001) Stable strontium accumulation by
860 earthworms: a paradigm for radiostrontium interactions with its cationic analogue,
861 calcium. *Environmental Toxicology and Chemistry* **20**, 1236-1243.
862 Morgan J. E., Richards S. P. G. and Morgan A. J. (2002) Contrasting accumulative patterns
863 of two cationic analogues, Ca and Sr, in ecophysiologically contrasting earthworm
864 species (*Aporrectodea longa* and *Allolobophora chlorotica*) from the field. *Applied*
865 *Soil Ecology* **21**, 11-22.
866 Morse, J.W., Wang, Q.W. and Tsio, M.Y. (1997) Influences of temperature and Mg:Ca ratio
867 on $CaCO_3$ preciptiates from seawater. *Geology* **25**, 85-87.
868 Mosselmans J. F. W., Quinn P. D., Dent A. J., Cavill S. A., Diaz-Moreno S., Peach, A.,
869 Leicester P. J., Keylock S. J., Gregory S., Atkinson K. D. and Roque Rosell J. (2009)
870 I18-the microfocus spectroscopy beamline at the Diamond Light Source. *Journal of*
871 *Synchrotron Radiation* **16**, 818-824.
872 Nahmani J., Hodson M. E. and Black, S. (2007) A review of studies performed to
873 assessmetal uptake by earthworms. *Environmental Pollution* **145**, 402-424.
874 Nehrke G., Reichart G., van-Capellen P., Meile C. and Bijma J. (2007) Dependence of
875 calcite growth rate and Sr partitioning on solution stoichiometry: Non-Kossel crystal
876 growth. *Geochimica et Cosmochimica Acta* **71**, 2240 - 2249.

877 Nickless E., Booth S. and Mosley P. (1976) The celestite resources of the north-east of
878 Bristol with notes on occurrences north and south of the Mendip Hills and in the Vale
879 of Glamorgan: Description of the 1:25000 resource sheet ST68 and parts of ST59,
880 69, 79, 58, 78, 67 and 77. In: Sciences, I. o. G. (Ed.), Edinburgh, UK.
881 Parkman R. H., Charnock J. M., Livens F. R. and Vaughan, D. J. (1998) A study of the
882 interaction of strontium ions in aqueous solution with the surfaces of calcite and
883 kaolinite. *Geochimica et Cosmochimica Acta* **62**, 1481-1492.
884 Perdrial N., Rivera N., Thompson A., O'Day P.A. and Chorover J. (2011) Trace contaminant
885 concentration ffects mineral transformation and pollutant fate in hydroxide-weathered
886 Hanford sediments. *Journal of Hazardous Waste* **197**, 119-127.
887 Piearce T.G. (1972) The calcium relations of selected *Lumbricidae*. *Journal of Animal*
888 *Ecology* **41**,167–188.
889 Pingitore Jr. N. E., Lytle F. W., Davies B. M., Eastman M. P., Eller, P. G. and Larson E. M.
890 (1992) Mode of incorporation of Sr^{2+} in calcite: Determination by X-ray absorption
891 spectroscopy. *Geochimica et Cosmochimica Acta* **56**, 1531-1538.
892 Radha, A.V, Fernandez-Martinez, A., Hu, Y., Young-Shin, J, Waychunas, G.A. and
893 Navrotsky, A. (2012) Energetic and structural studies of amorphous $Ca_{1-x}Mg_xCO_3.nH_2O$ ($0 \leq x \leq 1$). *Geochimica et Cosmochimica Acta* **90**, 83-95.
894
895 Ravel B. and Newville M. A. (2005) ATHENA, ARTEMIS, HEPHAESTUS: data analysis for
896 X-ray absorption spectroscopy using IFEFFIT. *Journal of Synchrotron Radiation* **12**,
897 537-541.
898 Raz, S., Weiner, S. and Addadi, L/ (2000) Formation of high-magnesian calcites via an
899 amorphous precursor phase: Possible biological implications. *Advanced materials*
900 **12**, 38-42.
901 Reis, J.B., Anderson, M.A. and Hill, R.T. (2008) Seawater Mg/Ca controls polymorph
902 mineralogy of microbial $CaCO_3$: A potential proxy for calcite-aragonite seas in
903 Precambrian time. *Geobiology* **6**, 106-119.

Riley R.G.; Zachara J.M. and Wobber F.J. (1992) Chemical contamiannts on DOE Lands and selection of contaminant mixture for subsurface science research. DOE/ER-0547T; U.S. Department of Energy, Office of Energy Research: Washington, DC,

Robertson J. D. (1963) The Function of the Calciferous Glands of Earthworms. *Journal of Experimental Biology* **13**, 279-297.

Rodriguez-Blanco J. D., Bots P., Rocal-Herrero T., Shaw S. and Benning L. G. (2011a) The role of Mg in the formation of monohydrocalcite *Mineralogical Magazine* **75**, 1741.

Rodriguez-Blanco J. D., Shaw S. and Benning L. G. (2011b) The kinetics and mechanisms of amorphous calcium carbonate (ACC) crystallization to calcite, via vaterite. *Nanoscale* **3**, 265-271.

Schofield P. F., Knight K. S., Covey-Crump S. J., Cressey G. and Stretton I. C. (2002) Accurate quantification of the modal mineralogy of rocks when image analysis is difficult. *Mineralogical Magazine* **66**, 189–200.

Shannon R. D. (1976) Revised effective ionic radii and systematic studies of interatomic distances in halides and chalcogenides. *Acta Crystallographica* **A32**, 751-767.

Shore M. and Fowler A. D. (1996) Oscillatory zoning in minerals; a common phenomenon. *The Canadian Mineralolgist* **34**, 1111-1126.

Sinclair D.J., Banner J.L., Taylor F.W., Partin J., Jenson J., Mylroie J. Goddard E. Quinn T., Jocson J. and Miklavic B. (2012) Magnesium and strontium systematics in tropical speleothems from the Western Pacific. *Chemical Geology* **294**, 1-17.

Solé V. A., Papillon E., Cotte M., Walter P. and Susini J. (2007) A multiplatform code for the analysis of energy-dispersive X-ray fluorescence spectra. *Spectrochimica Acta* **62**, 63-68.

Spycher N., Weathers T., Barkouki T., Smith R.W., Ginn T.R., Zhang G.X. Fujita Y., Wu Y.X., Ajo-Franklin J., hubbard S. and Sengor S.S. (2009) Remediation of Sr-90 by induced calcite precipitation: Reactive transport modelling on several fronts. *Abtracts of paper of the American Chemical Society **237,*** Abstract 114-GEOC

931 Standring W.J.F., Oughton D.H. and Salbu B. (2002) Potential remobilisation of Cs-137, Co-
932 60, Tc-99 and Sr-90 from contaminated Mayak sediments river and estuary
933 environments. *Environmental Science and Technology* **36**, 2330-2337.
934 Stipp S. L. and Hochella M. F. (1991) Structure and bonding environments at the calcite
935 surface as observed with X-ray photoelectron spectroscopy (XPS) and low energy
936 electron diffraction (LEED). *Geochimica et Cosmochimica Acta* **55**, 1723-1736.
937 Stoll H.M., Klaas C.M., Probert I., Encinar J.R. and Alonso J.I.G. (2002) Calcification rate
938 and temperature effects on Sr partitioning in coccoliths of multiple species of
939 coccolithophorids in culture. *Global and Planetary Change* **34**, 153_171
940 Tang J., Köhler S. J. and Dietzel M. (2008) Sr^{2+}/Ca^{2+} and $^{44}Ca/^{40}Ca$ fractionation during
941 inorganic calcite formation: I. Sr incorporation. *Geochimica et Cosmochimica Acta*
942 **72**, 3718-3732.
943 Tenderholt A. and Quinn P. (2009) PySpline. Free Software Foundation, Inc., Boston, USA.
944 Tertre E., Page J. and Beaucaire C. (2012) Ion exchange model for reversible sorption of
945 divalent metals on calcite: Implications for natural environments. *Environmental*
946 *Science and Technology* **46**, 10055-10062.
947 Tesoriero A. J. and Pankow J. F. (1996) Solid solution partitioning of Sr^{2+}, Ba^{2+}, and Cd^{2+} to
948 calcite. *Geochimica et Cosmochimica Acta* **60**, 1053-1063.
949 Thompson A., Steefel C.I., Perdrial N. and Chorover J. (2010) Contaminant desoprtion
950 during long-term leaching of hydroxide-weathered Hanford sediments. *Environmental*
951 *Science and Technology* **44**, 1992-1997.
952 Tomic S., Searle B. G., Wander A., Harrison N. M., Dent A., Mosselmans J. F. W. and
953 Inglesfield J. E. (2004) DL-EXCURV. STFC Daresbury Laboratory, Daresbury, UK.
954 Veizer J. (1983) Trace elements and isotopes in sedimentary carbonates. *Carbonates*
955 *Mineralogy and Chemistry; Reviews in Mineralogy* **11**, 265–299.
956 Versteegh E.A.A., Hodson M.E. and Black S. (2012) Earthworm secreted calcium carbonate
957 – a new palaeothermometer? 22nd Goldschmidt Conference, Montreal, Canada.
958 Abstract volume.

959 Wang, D., Hamm, L.M., Gluffre, A.J., Echigo, T., Rimstidt, J.D., de Yoreo, J.J., Grotzinger, J.
960 and Dove, P.M. (2012) Revisiting geochemical controls on patterns of carbonate
961 depostion through the lens of multiple pathways to mineralisation. *Faraday*
962 *Discussions* **159**, 371-386.
963 Warren L. A., Maurice P. A., Parmar N. and Ferris F. G. (2001) Microbially Mediated Calcium
964 Carbonate Precipitation: Implications for Interpreting Calcite Precipitation and for
965 Solid-Phase Capture of Inorganic Contaminants. *Geomicrobiology Journal* **18**, 93-
966 115.
967 Wassenburg J.A., Immenhauser A., Richter D.K., Jochum K.P., Fietzke J., Deininger M.,
968 Goos M., Scholz D., Sabaoui A. (2012) Climate and cave control on
969 Pleistocene/Holocene calcite-to-aragonite transitions in speleothems from Morocco:
970 Elemental and isotopic evidence. *Geochimica et Cosmochimica Acta* 92, 23-47.
971

Figure Captions

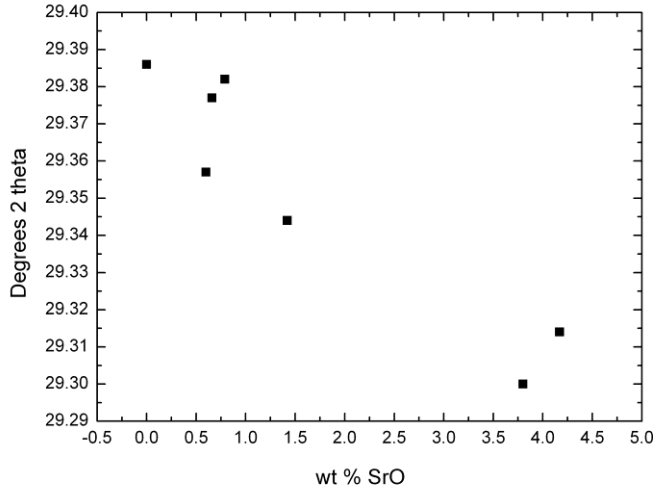

Figure 1. Plot of the calcite 104 peak position (λ = Cu Kα_1) as a function of average wt% SrO as estimated from point EPMA analyses across a core-rim line profile.

978 **Figure 2.** Optical images of granules produced by *L. terrestris* in Hamble soils amended with
979 various Sr concentrations showing the two general morphological types that the granules

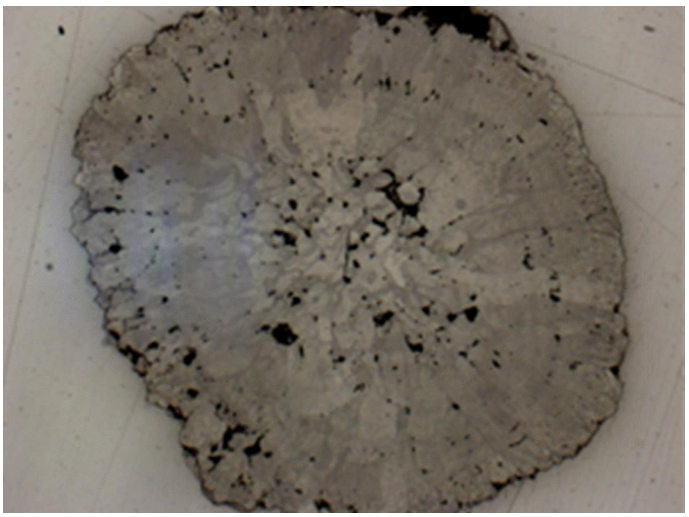

980 displayed. (a) is a granule from HS500
981 (b) is a granule from HS100. Granules are c. 2 mm in diameter.

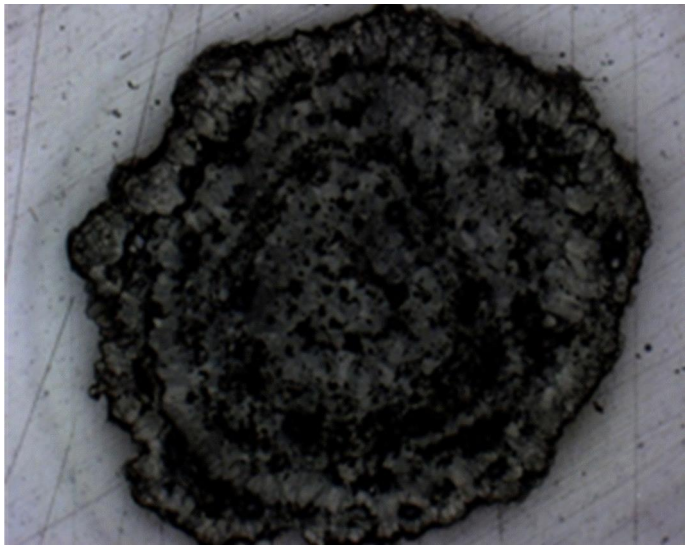

982
983
984

985

986 **Figure 3.** Sr distribution maps from EPMA of granules produced by *L. terrestris* in Hamble
987 soils amended with various Sr concentrations.
988 (a) a granule recovered from the depurate of earthworms kept in HS100

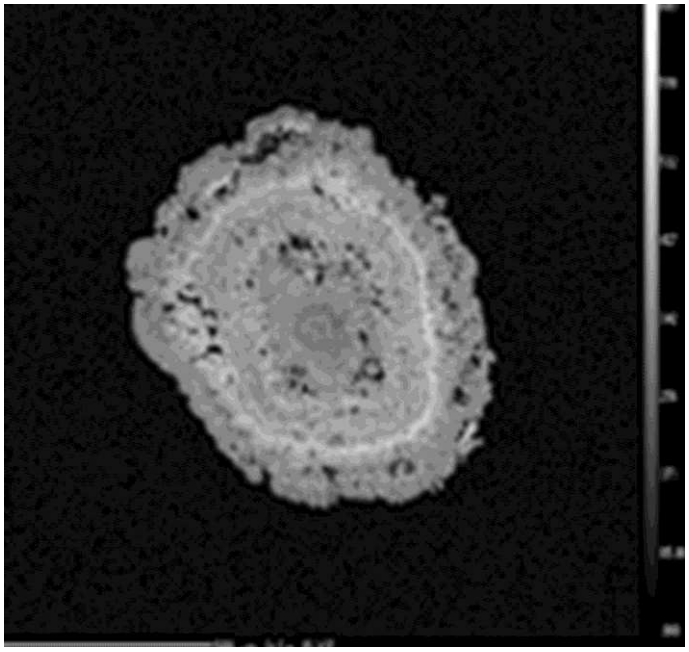

989
990
991 (b) a granule recovered from the depurate of earthworms kept in HS100

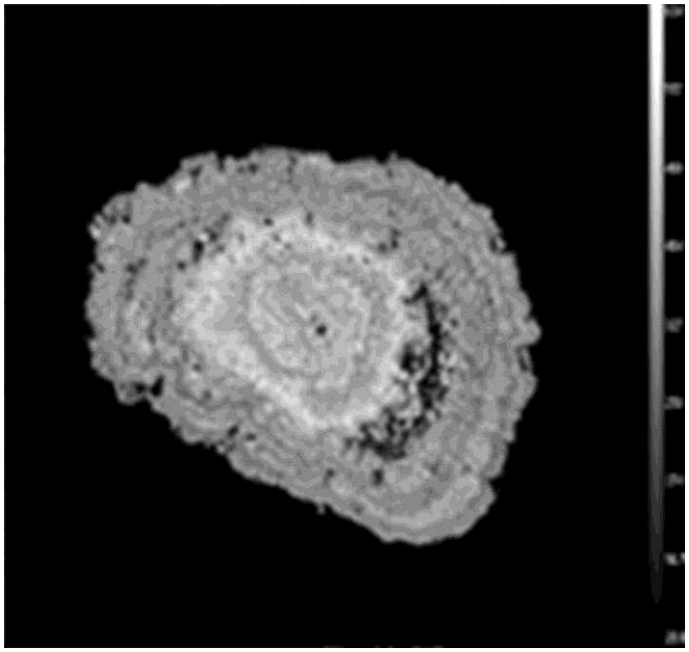

992
993
994

(c) a granule extracted from HS500 and

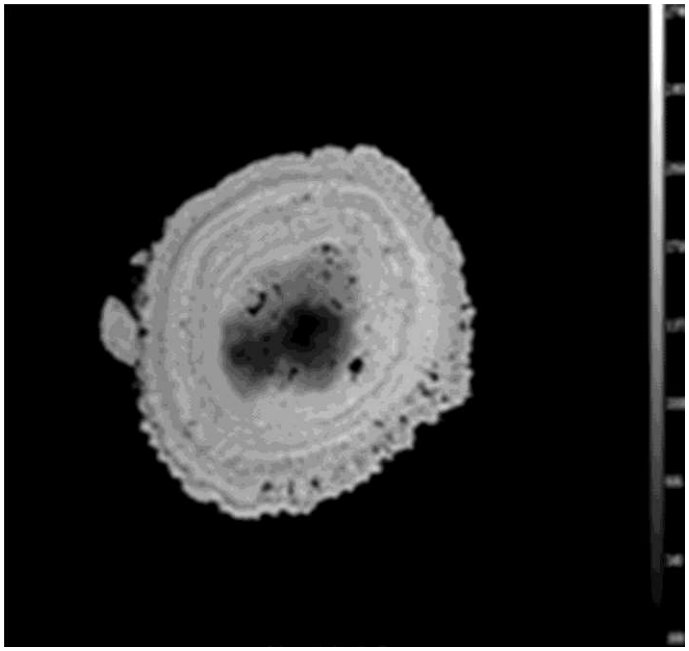

(d) a granule extracted from HS100.

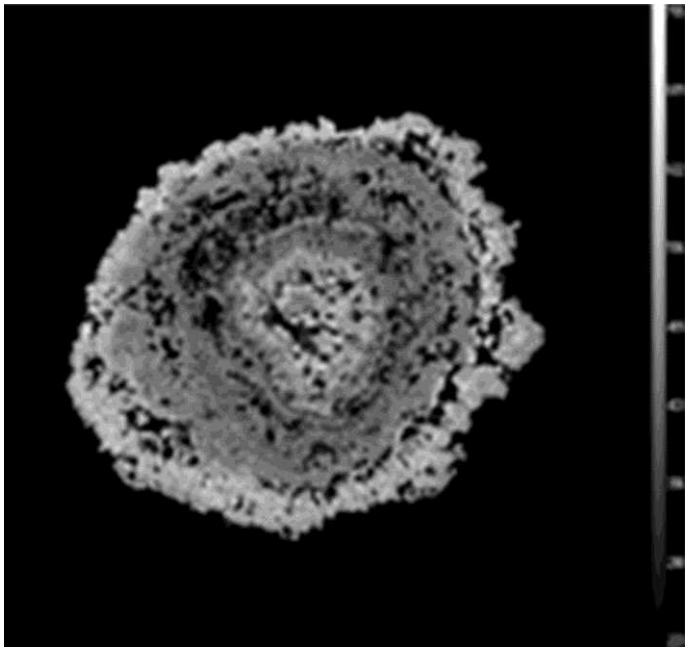

Figure 4. Mg and Mn distribution maps from EPMA of granules produced by *L. terrestris* in Hamble soils amended with various Sr concentrations.

(a) Mg map from a granule from HS150

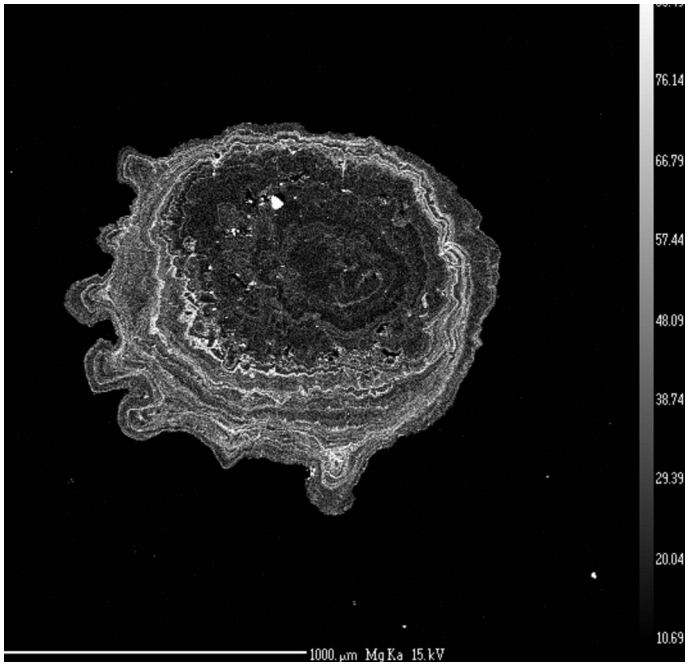

(b) Mg map of a granule from HS100

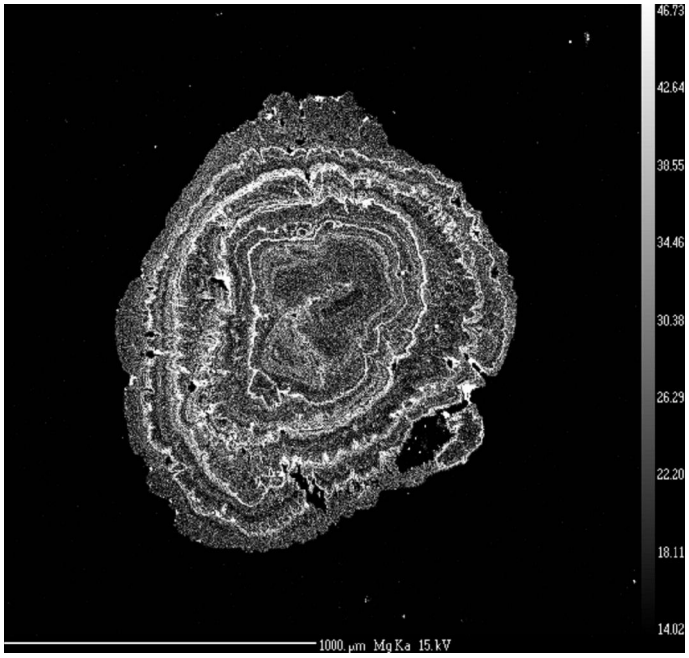

(c) Mn map of a granule recovered from the depurate of an earthworm kept in HS100 and

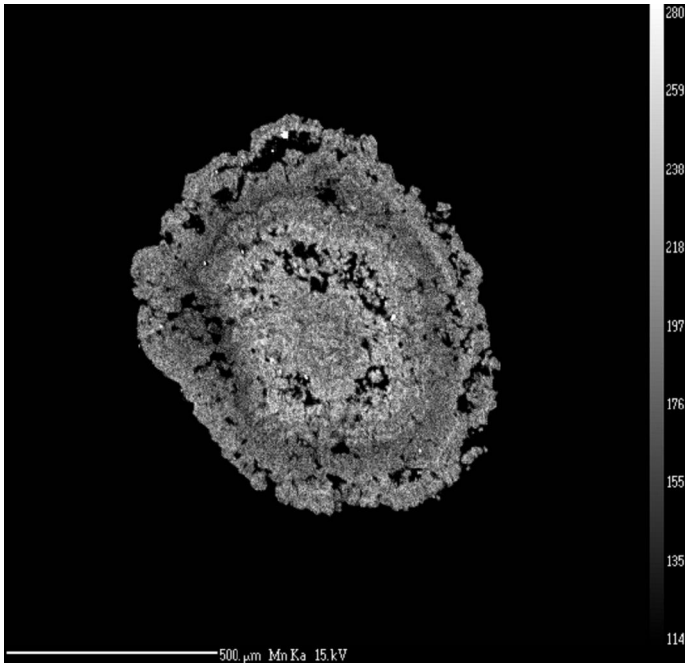

(d) Mn map of a granule from HS100.

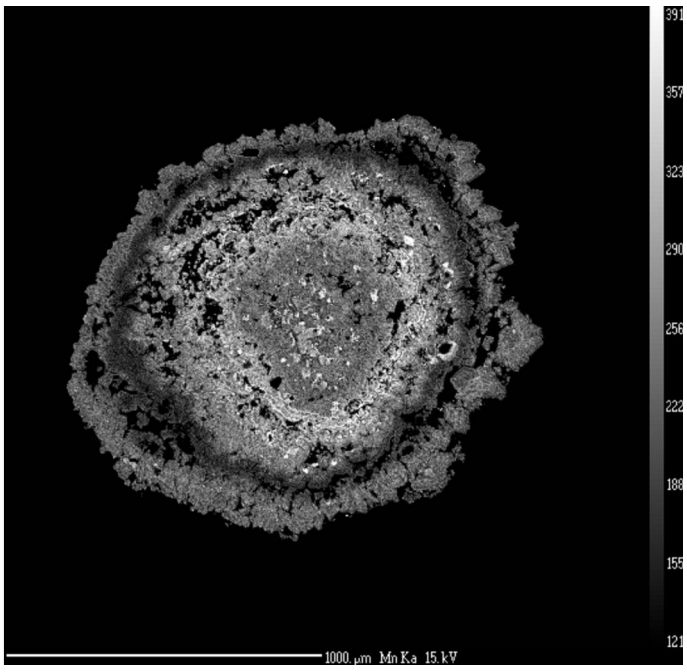

Figure 5. Ca K-edge XANES spectra for the carbonate standards: calcite (data from Fraser et al., 2011), Sr-bearing aragonite (obtained from Dr A. Finch, University of St Andrews) and synthetic vaterite (obtained from Dr P. Bots, University of Leeds) andfor selected points from individual granules extracted from HS100, YSL and YSH. The first derivative of the pre-edge and edge are shown in the inset. . “1”, “2”, “3” and “4” highlight diagnostic features of the spectra (see text for details).

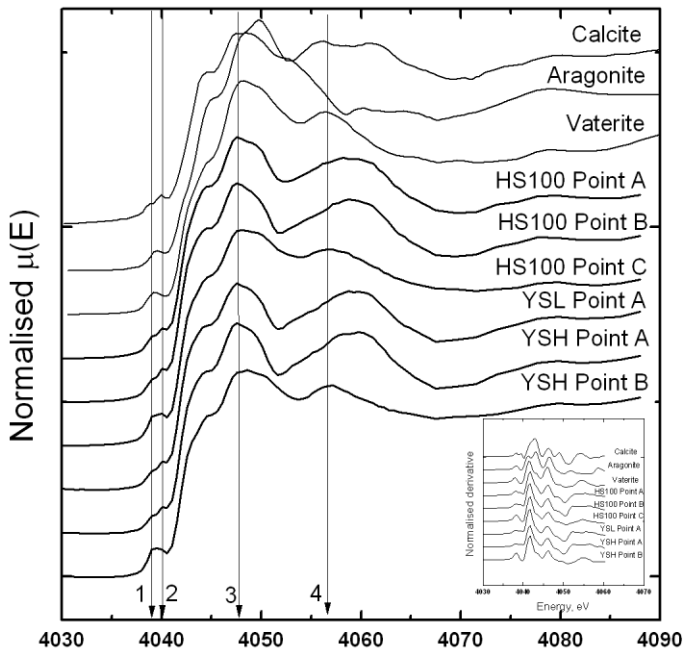

Figure 6. Sr K -edge XANES spectra for the Sr standards used in this study and for three points on a granule from HS100 (HS100 Points A to C), a point on a granule from YSL (YSL Point A) and two points on a granule from YSH (YSH Point A and B). Spectra were collected from the same points as those in Fig. 5. For the standards “Sr ads onto calcite” and “Sr ads onto granule” are for Sr adsorbed onto calcite and granules, respectively. “Vaterite copp with Sr” is for the synthetic vaterite co-precipitated with Sr.

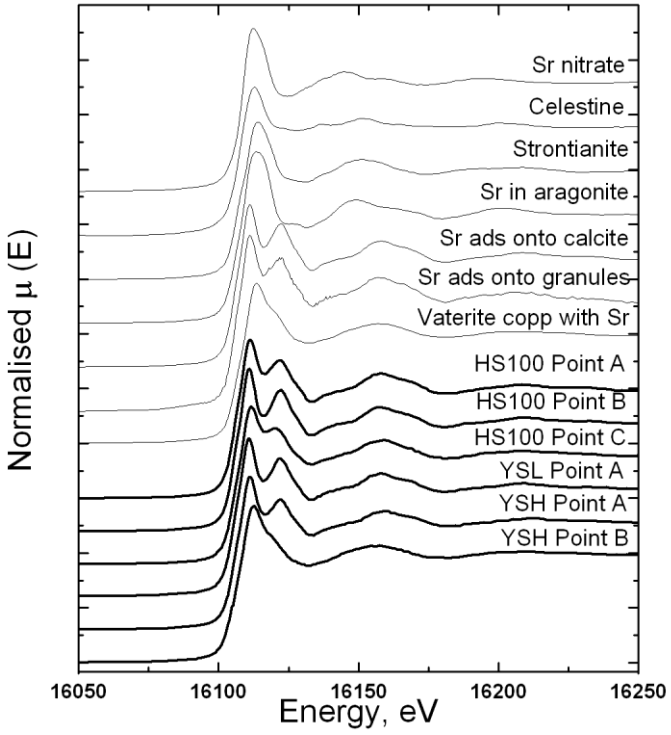

1031 **Figure 7.** k^3-weighted EXAFS spectra with EXAFS model (dotted line) for the same data as
1032 Fig. 6.

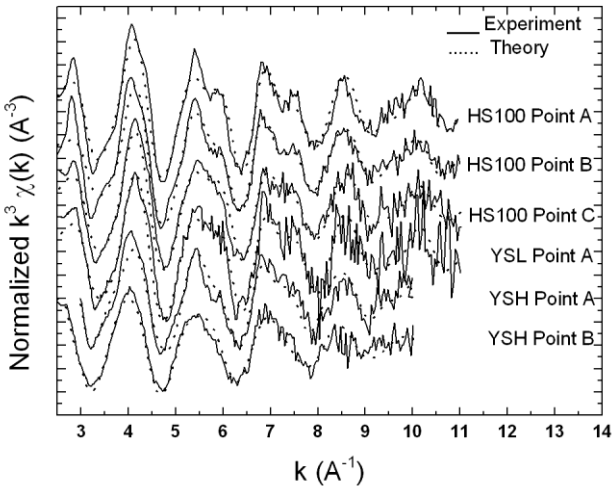

1033
1034

Table 1. Soil properties. Values are mean ± s.d. with number of replicates given in brackets.

Parameter /Soil	HS	HS50	HS100	HS150	HS500	YSL	YSH
pH	8.3 (n = 1)	8.18 ± 0.10 (n = 5)	8.24 ± 0.02 (n = 5)	8.24 ± 0.0 (n = 5)	8.05 ± 0.06 (n = 5)	5.62 ± 0.16 (n = 5)	8.06 ± 0.22 (n = 5)
WHC / % (n = 3)	39.9 ± 0.5	ND[a]	ND[a]	ND[a]	ND[a]	74.9 ± 0.2	51.4 ± 9.4
Organic matter content (LOI) / % (n = 1)	3.0	ND[a]	ND[a]	ND[a]	ND[a]	9.2	3.2
Target Sr concentration / mg kg^{-1}	-	50	100	150	500	-	-
Actual Soil Sr / mg kg^{-1}	32 ± 2 (n = 3)	72 ±6 (n = 5)	145 ± 42 (n=5)	180 ± 30 (n=5)	600 ± 50 (n=5)	950 ± 50 (n=5)	11000 ± 900 (n=5)
Soil Ca / mg kg^{-1}	8550 ± 990 (n = 3)	8 600 ± 400 (n = 5)	8 900 ± 500 (n = 5)	8 100 ± 400 (n = 5)	9 800 ± 300 (n = 5)	3 540 ± 240 (n = 5)	24 100 ± 800 (n = 5)
Soil solution Sr / mg L^{-1}	ND[a]	5.58 ± 1.35 (n = 5)	10.1 ± 2.79 (n = 5)	19.7 ± 1.96 (n = 5)	131 ± 25.28 (n = 5)	21.9 ± 10.9 (n = 5)	80.8 ± 11.6 (n = 5)
Soil solution Ca / mg L^{-1}	ND[a]	288 ± 81	298 ± 55	359 ± 117	790 ± 49	95 ± 44	228 ± 38

[a]ND = Not determined, property assumed to be unaffected by addition of Sr salt to Hamble soil

Table 2. Earthworm and granule data. Values either represent mean values ± s.d. (n = 5) or, for granules, single values derived from the combining of all 5 replicates to give sufficient mass for accurate measurement and analysis.

Parameter /Soil	HS	HS50	HS100	HS150	HS500	YSL	YSH
Earthworm Sr / mg kg^{-1}	13.6 ± 6.10	69.1 ± 17.1	179 ± 83.5	213 ± 36.5	708 ± 112	603 ± 92.9	4100 ± 1070
Earthworm Ca / mg kg^{-1}	10600 ± 1500	10500 ± 1980	11900 ± 4300	9550 ± 1960	11300 ± 1600	6100 ± 508	11300 ± 1500
Granule Sr / mg kg^{-1}	345 ± 23[a]	4000	7930	12000	34200	14700	51400
Granule Ca mg kg^{-1}	ND	425000	449000	427000	447000	338000	402000
Production rate / mg $CaCO_3$ g_{worm}^{-1} day^{-1}	0.28	0.47	0.38	0.32	0.48	0.05	0.19
Production rate / mg $CaCO_3$ $earthworm^{-1}$ day^{-1}	1.52	0.89	1.50	1.67	2.30	0.26	0.74

[a]values taken from Hamble soil data, Lee et al. (2008)

Table 3. Distribution coefficients for Sr and Ca partitioning. Values for soil and soil solution distribution coefficients are mean values ± s.d. (n = 5). For granules, single values based on the mean soil, soil solution and earthworm concentrations of Sr and Ca and the Sr and Ca concentrations in the pooled granules from all 5 replicates are given.

Components / Soil	HS	HS50	HS100	HS150	HS500	YSL	YSH
Earthworm / soil	0.58 ± 0.22	0.79 ± 0.10	1.01 ± 0.43	1.05 ± 0.29	1.04 ± 0.19	0.37 ± 0.05	0.78 ± 0.09
Earthworm / soil solution	ND	0.36 ± 0.06	0.42 ± 0.19	0.41 ± 0.06	0.38 ± 0.06	0.44 ± 0.05	1.01 ± 0.16
Granule / soil	ND	1.12	1.09	1.27	1.25	0.16	0.28
Granule / soil solution	ND	0.50	0.50	0.51	0.46	0.19	0.36
Granule / earthworm	ND	1.43	1.17	1.26	1.22	0.44	0.35

Table 4. The calcium carbonate mineralogy as identified by XRD (XRD-NHM and μXRD-NHM) and the trace element chemistry from EPMA of granules. The calcite 104 peak 2θ position is provided based upon the wavelength of Cu $K\alpha_1$ radiation. The average wt% SrO, MgO and MnO levels are taken from EPMA analyses within a rim-to-core line profile.

Sample name	Carbonate phases identified	Calcite 104 peak 2θ (XRD-NHM)	Range of SrO concentrations	Average wt % SrO	Range of MgO concentrations	Average wt % MgO	Range of MnO concentrations	Average wt % MnO
HS control	calcite, vaterite	29.386(2)	0	0.04[a]	-	0.06[a]	-	0.02[a]
HS50	calcite, vaterite	29.357(2)	0.48-0.83	0.60	0.04-0.017	0.08	0.20-0.39	0.30
HS100	calcite, vaterite	29.377(2)	0.10-1.58	0.66	0.06-0.23	0.12	0.05-0.55	0.22
HS100 FRESH[b]	Calcite	29.382(2)	0.56-1.14	0.79	0.02-0.17	0.07	0.19-0.41	0.30
HS150	Calcite	29.344(2)	0.97-1.99	1.42	0.02-0.33	0.10	0.02-0.45	0.23
HS150 FRESH[2]	Calcite	29.314(2)	3.49-5.04	4.17	0.01-0.10	0.05	0.01-0.07	0.04
HS500	Calcite	29.301(2)	0.11-4.91	3.85	0.02-0.19	0.07	0.01-0.07	0.04
YSL	calcite, vaterite	29.352(2)	0.08-0.29	0.12	0.08-0.19	0.14	0.03-0.10	0.06
YSH	calcite, vaterite	29.352(2)	0.07-0.19	0.13	0.12-0.28	0.19	0.01-0.08	0.04

[a] values taken from Lee et al. (2008)

[b] FRESH refers to granules collected from earthworm depurate at the end of the experiment rather than those recovered from the bulk soil by sieving

Table 5. Table summarising XAS fits for the selected points on a granules produced by *L. terrestris* in HS100, YSL and YSH together with relevant standards

Point/Std	Notes	Scattering Atom	Coordination Number	Interatomic distance (Å)	Debye-Waller factor ($Å^2$)	Fit Index
Sr in HS100 Point A	High Sr in the centre of the granule	O C Ca Ca	6 6 6 6	2.51(±0.02) 3.38(±0.06) 4.09(±0.02) 5.04(±0.06)	0.013(±0.002) 0.040(±0.017) 0.024(±0.005) 0.032(±0.017)	28.7
Sr in HS100 Point B	Low Sr on the edge of the granule	O C Ca Ca	6 6 6 6	2.52(±0.01) 3.35(±0.03) 4.10(±0.04) 5.04(±0.07)	0.014(±0.002) 0.030(±0.011) 0.029(±0.008) 0.027(±0.009)	34.9
Sr in HS100 Point C	Medium Sr near a rim	O C Ca Ca	6 6 6 6	2.51(±0.01) 3.36(±0.06) 4.10(±0.04) 5.02(±0.07)	0.012(±0.003) 0.049(±0.027) 0.036(±0.065) 0.044(±0.022)	31.5
Sr in YSL Point A	Medium Sr near the edge of the granule	O C Ca Ca	6 6 6 6	2.50(±0.01) 3.32(±0.08) 4.10(±0.06) 5.02(±0.14)	0.013(±0.004) 0.035(±0.025) 0.024(±0.007) 0.040(±0.028)	39.5
Sr in YSH Point A	High Sr on a hotspot top left side of the granule	O C Ca Ca	6 6 6 6	2.53(±0.02) 3.29(±0.11) 4.08(±0.06) 5.01(±0.09)	0.017(±0.004) 0.030(±0.017) 0.037(±0.050) 0.034(±0.036)	33.7
Sr adsorbed onto granule		O C Ca Ca	6 6 6 6	2.52(±0.02) 3.40(±0.19) 4.10(±0.07) 5.02(±0.06)	0.008(±0.006) 0.048(±0.082) 0.028(±0.017) 0.019(±0.027)	33.0
Sr in YSH Point B	Medium Sr	O C Ca	8.2 5.2 3.5	2.55(±0.01) 2.95(±0.10) 4.13(±0.06)	0.025(±0.005) 0.035(±0.025) 0.040(±0.019)	29.3
Sr adsorbed onto calcite		O C Ca Ca	6 6 6 6	2.51(±0.01) 3.33(±0.11) 4.07(±0.03) 5.00(±0.04)	0.010(±0.004) 0.008(±0.017) 0.022(±0.010) 0.008(±0.007)	31.7
Vaterite co-precipitated with Sr		O C Ca	8 5.7 4.4	2.55(±0.01) 2.94(±0.15) 4.17(±0.04)	0.022(±0.003) 0.035(±0.022) 0.043(±0.014)	23.8